Supplementary Materials for

Measurement of Gene Regulation in Individual Cells Reveals Rapid Switching Between Promoter States

Leonardo A. Sepúlveda, Heng Xu, Jing Zhang, Mengyu Wang and Ido Golding.

correspondence to: golding@bcm.edu, igolding@illinois.edu

This PDF file includes:

Other Suplementary Materials for this manuscript includes the following:

Materials and Methods

1 Experimental protocols

1.1 Bacterial strains and plasmids

All bacterial strains and plasmids are listed in **table S1**.

1.2 Growth media and conditions

Unless otherwise stated, all strains were grown in LB (1 L of medium contains 10 g tryptone (BD Biosciences,), 5 g yeast extract (BD Biosciences), 5 g NaCl (Fisher Scientific) and 1 ml 1 M NaOH (Fisher Scientific)) at 37 °C with shaking (265 rpm). Cultures from fresh colonies were grown overnight (14-16 hours) in 2 ml of medium in the presence of antibiotics when appropriate (30 µg/ml Ampicillin (Fisher Scientific) and 50 µg/ml Kanamycin (Fisher Scientific) for AP326, AP327, AP365 and AP366; 34 µg/ml of Chloramphenicol (Fisher Scientific) and 50 µg/ml Kanamycin for LSG03; and 15 µg/ml Kanamycin for DH5αZ1(pZS21-*cIyfp*)). Overday cultures for each experiment were grown as described below.

1.2.1 Antibody washing. 5 ml of LB were inoculated with a colony of NK7049 and grown overnight. The overnight culture was then split between two 2-L flasks (2.5 ml to each flask) containing 250 ml LB and grown to $OD_{600} \approx 1$. Next, the cultures were pooled, and a total of 480 ml was distributed into 12 ice-cold 50-ml centrifuge tubes (40 ml/tube). Each sample was then treated according to the procedures described in **section 1.4**.

1.2.2 Immunofluorescence, single molecule fluorescence in situ hybridization (smFISH), and combined immunofluorescence and smFISH (IF-smFISH) of lambda lysogens. Overnights of NK7049 or MG1655 (negative controls), and NK7049λ_{WT} or MG1655λ_{831} (lysogens) were diluted 1:1000 in 25 ml of LB and grown in 250-ml baffled flasks to $OD_{600} \approx 0.3$. Each sample was then treated according to the procedures described in **sections 1.3**, **1.5** or **1.6**.

1.2.3 Immunofluorescence of CI-YFP reporter. An overnight of DH5αZ1(pZS21-*cIyfp*) was used to prepare 6 cultures, 20 ml LB each, at dilutions ranging from 1:100 to 1:1500, such that they reached $OD_{600} \approx 0.1$ at 30 min intervals. Cells were grown at 32 °C, and when a culture reached $OD_{600} \approx 0.1$, cells were centrifuged at 4500g for 5 min

and resuspended in 1 ml of pre-warmed LB containing 100 ng/ml anhydrotetracycline (Clontech). The culture was then moved to a microcentrifuge tube and mixed for 3 min in a nutator. Cells were centrifuged at ~20000g for 30 sec, the supernatant was removed and the cells were washed twice (resuspended in 1 ml of prewarmed LB and then centrifuged at ~20000g for 30 sec). A fraction of the cells was then diluted again in 20 ml of prewarmed LB medium. The dilution ratios (1:1250 to 1:40) were chosen such that all 6 cultures would reach $OD_{600} \approx 0.1$ at approximately the same time. Thus, all samples were induced for the same amount of time (3 min), but cells in each sample underwent a different number of cell divisions after induction. As a result, at the time of harvesting each sample exhibited different CI-YFP expression levels. 1/6 of each DH5αZ1(pZS21-*cIyfp*) culture was then transferred to an ice-cold 50-ml centrifuge tube. To image single CI-YFP molecules, we performed the experiment as above, but induced only a single culture, using 5 ng/ml anhydrotetracycline, and the culture was then transferred to an ice-cold 50-ml centrifuge tube. As negative control, an overnight of MG1655 was diluted 1:1000 in 25 ml of LB. Cells were then grown in 250-ml baffled flasks to $OD_{600} \approx 0.1$, and the culture transferred to an ice-cold 50-ml centrifuge tube. Each sample was then treated according to the procedure described in **section 1.3**.

1.2.4 IF-smFISH of P_{RM} reporter strains. Overnight cultures of AP365 (O_L^+) or AP326 (O_L^-) were diluted 1:1000 in 25 ml of LB containing 30 µl/ml Ampicillin, 50 µl/ml Kanamycin and 1mM of isopropyl β-D-1-thiogalactopyranoside (IPTG, Sigma) to induce the production of CI. Every time the culture reached $OD_{600} \approx 0.3$, it was divided in half. One half was diluted into fresh, pre-warmed LB medium with antibiotics and IPTG, while a fraction of the other half of the culture (first $1/2^5$, then $1/2^4$, up to 1/2) was centrifuged at ~20000g for 30 sec, resuspended into medium without inducer, and grown in parallel. Thus, cells in each sample underwent a different number of cell divisions in a non-induced state. As a result, at the time of harvesting, each sample exhibited different CI expression levels. 1/6 of each culture was then transferred to an ice-cold 50-ml centrifuge tube. As a negative control, overnights of NK7049 were diluted 1:1000 in 25 ml of LB. Cells were then grown in 250 ml baffled flasks to $OD_{600} \approx 0.3$, and the culture transferred to an ice-cold 50-ml centrifuge tube. Each sample was then treated according to the procedure described in **section 1.6**.

1.2.5 Live imaging of the galK locus. Overnight cultures of LSG03 were diluted 1:1000, grown in the presence of 10 µM salicylate (Sigma) to $OD_{600} \approx 0.2$, centrifuged and prepared for imaging according to the procedure described in **section 1.7**.

1.3 Immunofluorescence

Unless otherwise stated, all steps were carried out at room temperature, cells were centrifuged at 4500g for 5 min, and washes were performed as follows: Cell pellets were resuspended in 1 ml 1×PBS, centrifuged and the supernatant was removed.

1.3.1 Cell harvesting and sample fixation. Cells were grown as described in **section 1.2**. Next, cells were centrifuged at 4 °C, the supernatant was decanted and the remaining liquid was removed by tapping the inverted tube into a paper towel. The cell pellet was then resuspended in 1 ml of ice-cold 3.7% formaldehyde (Fisher Scientific) in 1×PBS (Fisher Scientific), transferred to a microcentrifuge tube and mixed for 30 min using a nutator.

1.3.2 Ethanol permeabilization. Next, cells were centrifuged and the supernatant was removed. Cells were washed twice. The cell pellet was resuspended in 300 µl of water. 700 µl of ethanol was added for a final concentration of 70% ethanol. Finally, cells were mixed for 1 hr using a nutator.

1.3.3 Lysozyme permeabilization. Cells were centrifuged and the supernatant removed. The cell pellet was resuspended in 1 ml of 25 µg/ml lysozyme (Sigma) in 1×TE (Sigma) and the cell suspension was mixed for 10 min using a nutator. The cells were then centrifuged at ~20000g for 30 sec and the supernatant was removed. Finally, cells were washed three times in 1×PBS. Each time, the cells were centrifuged at ~20000g for 30 sec.

1.3.4 Antibody incubation. Cells were resuspended in 100 µl of 2% blocking solution (10 ml of 2% blocking solution contain 1 ml 10×PBS, 0.2 g BSA (Sigma), and 5 µl Tween 20 (Fisher Scientific)) and incubated for 15 min. The cell suspension was then transferred to a new microcentrifuge tube. Cells were centrifuged at 4500g for 3 min and the supernatant was removed. Cells were then resuspended in 100 µl of primary antibody solution (**section 1.4**) in 2% blocking solution and mixed for 1 hr in a nutator. The cell suspension was transferred to a new microcentrifuge tube. Cells were centrifuged at 4500g for 3 min and the supernatant removed. Cells were washed twice. Next, cells were resuspended in 100 µl of secondary antibody solution, which was a 1:100 dilution of secondary antibody in 2% blocking solution (To label CI, we used Alexa488 goat anti-rabbit; to label CI-YFP, we used Alexa594 donkey anti-rabbit or Alexa647 goat anti-rabbit (all from Molecular Probes)). Finally, the tube was wrapped in aluminum foil, and the cell suspension was mixed for 1 hr in a nutator.

1.3.5 DNA staining. The cell suspension was transferred to a new microcentrifuge tube. Cells were centrifuged at 4500g for 3 min and the supernatant was removed. Cells were washed once. The cell pellet was then resuspended in 1ml 1×PBS with 10 µg/ml of 4',6-diamidino-2-phenylindole (DAPI, Sigma), and the cells were mixed for 10 min in a nutator. Cells were then centrifuged, the supernatant was removed, and the cell pellet was resuspended in 100 µl of 1×PBS. Cells were then imaged as described in **section 1.7**.

1.4 Antibody washing

To label the CI protein, we used a dried-down CI antiserum from rabbit (a gift from K. Shearwin, The University of Adelaide). Using a 1:100 dilution of this serum directly

in non-lysogenic cells (NK7049, where no CI is expressed) yielded a high fluorescence signal, due to non-specific binding of the primary antibody (**fig. S1**). To decrease the level of non-specific binding, we incubated the whole serum solution with non-lysogenic cells. The cells were then centrifuged, and the supernatant was used for our immunofluorescence experiments. Non-lysogenic cells labeled with pretreated serum showed very low non-specific binding, while lysogenic cells retained strong labeling (**Fig. 2A**). The antibody washing procedure is described below. Unless otherwise stated, steps were carried out at room temperature, and centrifugation steps were performed at 4500g for 5 min at 4 °C.

1.4.1 Cell harvesting and sample fixation. Cells were grown as described in **section 1.2**. The cell pellets were resuspended in 5 ml of of ice-cold 3.7% formaldehyde solution in 1×PBS. Each three tubes were pooled into one, ending up with 4 tubes, with 15 ml of solution each. Next, 5 ml of formaldehyde solution was added to each tube, and the tubes were mixed for 30 min in a nutator.

1.4.2 Ethanol permeabilization and lysozyme permeabilization. These steps were performed as described in **sections 1.3.2** and **1.3.3**, scaling the volume of washes and incubations by 20×.

1.4.3 Antibody incubation. After the last step of cell-wall permeabilization, each cell pellet was resuspended in 1 ml of RNAase-free 2% blocking solution (10 ml of 2% RNAse-free blocking solution contain 1 ml 10×PBS (Ambion), 0.2 g BSA, 5 µl Tween 20 and 100 µl 200 mM Ribonucleoside Vanadyl Complex (New England Biolabs)). The cell suspensions were then pooled, transferred to 8 microcentrifuge tubes (~500 µl/tube) and incubated at room temperature for 15 min. Cells were then centrifuged at ~20000g for 2 min and the supernatant was removed. Cells were mixed with 100 µl of 0.8% blocking solution with antibodies (1 ml of 0.8% blocking solution contains 160 µl Ultrapure BSA (Ambion), 100 µl 10×PBS, 0.5 µl Tween 20, 10 µl 200 mM Ribonucleoside Vanadyl Complex and 10 µl CI antiserum) and mixed for 1 hr in a nutator. Cells were centrifuged twice at ~20000g for 2 min and the supernatant was collected into a microcentrifuge tube. The resulting primary antibody solution was centrifuged once more at ~20000g for 2 min, and the supernatant transferred to a new microcentrifuge tube. 100 µl of this supernatant was used for incubation with primary antibodies, as described in **section 1.3**.

1.5 Single molecule fluorescence *in situ* hybridization (smFISH)

Probe design, probe labeling and *in situ* hybridization were performed as previously described (*25*). In brief, antisense oligonucleotide probes (48 probes for *cI* and 72 probes for *lacZ*, (*29*)) were designed and ordered with a 3' amine modification (Biosearch). The probes were pooled and then covalently coupled to 6-TAMRA (Invitrogen) and later purified using ethanol precipitation. Cells were grown as described in **section 1.2**, fixed, and permeabilized using ethanol. Cells were then incubated with fluorescently labeled

probes, washed, and the cellular DNA labeled using DAPI. Cells were then imaged as described in **section 1.7**.

We note that fixation is expected to "freeze" the state of the *E. coli* cell within ~1 min (*33*). We verified that this is indeed the case under our experimental conditions, by measuring the kinetics of mRNA degradation following rifampicin treatment (*34*) (**fig. S17**). We found that the measured kinetics agreed very well with the theoretical expectation (*35*), and we did not observe any delay that can be attributed to the fixation step.

1.6 Combined immunofluorescence and single molecule fluorescence *in situ* hybridization (IF-smFISH)

Simultaneous labeling of proteins and RNA was achieved by performing a modified version of the smFISH protocol (*25*) followed by sections of the immunofluorescence protocol, as described below. To protect the integrity of mRNA, we performed all steps using sterile, RNAse and DNAse-free aerosol-barrier pipet tips (Fisher Scientific); cleaned work areas with RNAseZap (Ambion) prior to every experiment; and used RNAse and DNAse-free reagents whenever possible. All aqueous solutions were prepared using Diethylpyrocarbonate (DEPC)-treated water (Ambion). Unless otherwise stated, steps were carried out at room temperature, and all centrifugation steps were performed at 4500g for 5 min.

1.6.1 Cell harvesting, sample fixation and ethanol permeabilization. Cells were grown as described in **section 1.2**. Fixation and ethanol permeabilization were carried out as in **section 1.3**, but using RNAse-free reagents.

1.6.2 Probe hybridization and washing. Cells suspended in 70% ethanol were centrifuged and the supernatant was removed. Cells were then resuspended in 10% wash solution (10 ml 10% wash solution contain 1 ml of 20×SSC (Ambion) and 1 g of formamide (Ambion)) and mixed for 5 min using a nutator. Meanwhile, a tube with 10% hybridization solution (10 ml of 10% hybridization solution contains 1 ml of 20×SSC, 1 g of formamide, 1 g of dextran sulfate (Sigma), 10 mg of *E. coli* tRNA (Sigma), 100 µl of 200 mM ribonucleoside-vanadyl complex and 40 µl of 50 mg/ml ultrapure BSA) was brought from -20 °C to room temperature and mixed thoroughly. Then, 50 µl of hybridization solution were moved to a new microcentrifuge tube, and 3.6 µl of 15 µM *lacZ* or *cI* probes were added, for a final probe concentration of 1 µM. Cells were centrifuged and the supernatant was removed. The pellet was resuspended in 50 µl of 10% hybridization solution with probes. The tube was wrapped in aluminum foil and incubated overnight in the dark at 30 °C. The next morning, the whole hybridization solution with cells (50 µl) was transferred to a new microcentrifuge tube covered in aluminum foil. 1 ml of 10% wash solution was added to the tube, and incubated for 5 min. Cells were then centrifuged, and the supernatant was removed. Cells were resuspended in 1 ml of 10% wash solution and then were incubated for 10 hr in the dark

at 30 °C. Cells were centrifuged and the supernatant was removed. The cell pellet was resuspended in 1 ml of 10% wash solution, and then was incubated for 14 hr in the dark at 30 °C.

1.6.3 Lysozyme permeabilization, antibody incubation and DNA staining. All remaining steps were performed as in the immunofluorescence protocol (**section 1.3**), but using RNAse-free water, PBS and 2% blocking solution.

1.7 Microscopy

1.7.1 Optical setup. We imaged cells under an inverted epifluorescence microscope (Nikon, Eclipse T*i*) with motorized stage control (Prior, Proscan III), universal specimen holder, and a motorized optical shutter to control fluorescence illumination exposure time (Sutter Instruments, SmartShutter). We used a mercury lamp as a light source (Nikon, Intensilight C-HGFIE), and band-pass filter cubes (Nikon; YFP, GFP, TexasRed and DAPI filter sets) for spectral separation. Imaging was performed using a 100×, NA 1.40, oil-immersion phase-contrast objective (Nikon, Plan Apo 100×/1.40 oil) combined with a ×2.5 lens located in front of a cooled EMCCD camera (Photometrics, Cascade II: 1024). For single-molecule characterization of the antibody labeling stoichiometry, we used an inverted epifluorescence microscope (Nikon, Eclipse T*i*) with a TIRF illuminator and a TIRF objective (Nikon, Apo TIRF 100×/1.49 oil). As a light source, we used a monolithic laser combiner (MLC400B, Agilent technologies), using the laser lines at 488 nm and 647 nm. Images were acquired with a cooled EMCCD camera (Andor, iXon Ultra 897). Both microscopes were installed on an optical table (TMC, breadboard and four-post support), and controlled using the Nikon Elements software (Nikon).

1.7.2 Imaging. Cells were prepared for imaging as previously described (*25*). The sample was then placed onto the microscope's slide holder, and the cells located using the phase-contrast channel. Images were taken at 9 z-positions separated by 200 nm. In all experiments, we used a 100 ms exposure for phase-contrast images. For fluorescence imaging (YFP, Alexa488, 6-TAMRA, Alexa594 and DAPI), we used exposure times between 0.2 and 3.2 s, with EM gain of 2000 to 3200. For single molecule imaging of CI-YFP molecules, coverslips were cleaned using the method described in (*36*). 10 s exposure time was used when imaging in the YFP channel. Images were acquired at multiple slide positions (to image a total of 300 to 3000 cells, typically 10 to 100 positions were needed).

2 Data analysis

2.1 Cell segmentation

We used Schnitzcells (*37*) to recognize cells in phase-contrast images of smFISH or live-cell samples. Images of samples labeled using immunofluorescence or IF-smFISH were segmented using a custom thresholding routine implemented in MATLAB (The Mathworks, Natick, MA). In brief, for each phase contrast z-stack, the best-focus image was identified by selecting the image with highest contrast (highest variance in pixel intensity) and the results were verified by visual inspection. Then, a pixel intensity threshold was manually selected using a custom MATLAB GUI. The preliminary segmentation masks produced either by Schnitzcells or by thresholding were later refined manually using the Schnitzcells GUI.

2.2 Spot quantification

We used Spatzcells (*25*) to quantify the intensity of spots in fluorescence images from immunofluorescence, smFISH, IF-smFISH or the *galK* locus reporter. Briefly, Spatzcells recognizes fluorescent spots within image z-stacks and locates, for each spot, the focal plane where the spot has the highest intensity. The intensity profile in a small "fitting region" around each spot is fitted to one or more two-dimensional elliptical Gaussians, based on the number of detected peaks inside the region, plus a tilted plane, of the form:

$$s(x,y)=\sum_{i=1}^{n} A_i e^{-\left[a_i(x-x_i)^2+b_i(y-y_i)^2+2c_i(x-x_i)(y-y_i)\right]}+B_0+B_x\left(x-x_0\right)+B_y\left(y-y_0\right). \qquad (1)$$

where n is the number of Gaussians used in the fit, (x_i,y_i) are the coordinates of each Gaussian, A_i is the amplitude (peak height) of each Gaussian and a_i, b_i and c_i are parameters describing the shape (minor and major axis) and orientation (angle of the major axis respect to the x-y axis) of each Gaussian. (x_0,y_0) are the coordinates at the center of the fitting region, whose background fluorescence is described by a plane with parameters B_0, B_x and B_y. Visual inspection of the fitting results showed a good agreement with the original images for both single-Gaussian and multi-Gaussian fits, in both protein and mRNA samples (**fig. S3**). The fitting parameters for the individual spots, in particular the total spot intensity (volume under the Gaussian, defined as $I=A_i\pi/\sqrt{a_ib_i-c_i^2}$) and the peak height (A_i) were used in the subsequent analysis after allocating each spot to the corresponding cell using the segmentation masks generated as described in **section 2.1**.

2.3 Protein quantification

2.3.1 Estimating the fluorescence of a single CI molecule using spot quantification. Protein spots in immunofluorescence images of non-lysogenic, lysogenic and P_{RM} reporter cells (either from the immunofluorescence protocol alone or combined with smFISH) were quantified using Spatzcells (**section 2.2**). The spot intensity histograms of lysogenic or P_{RM} reporter cells were fitted to a sum of six Gaussian functions of the form:

$$f_{\mathrm{protein}}(I) = \sum_{i=1}^{2} \varphi_i e^{-\frac{(I-\delta_i)^2}{2\varepsilon_i^2}} + \sum_{i=1}^{4} \phi_i e^{-\frac{(I-i\beta_{protein})^2}{2i\gamma_{protein}^2}}. \qquad (2)$$

The first term on the right-hand side corresponds to non-specific binding of antibodies, while the second term corresponds to binding of antibodies to CI molecules. The parameters (δ_i, ε_i) were obtained by fitting the spot intensity histogram of the non-lysogenic cells to the first term only. Nonspecific binding was usually not evident in protein spot histograms of lysogen or P_{RM} reporter samples labeled using immunofluorescence alone (**fig. S4A**) but it was evident in samples labeled using IF-smFISH (**fig. S10A**). The parameters ($\beta_{protein}$, $\gamma^2_{protein}$) are the mean and variance of the fluorescence intensity for the most abundant CI species in the sample. For lysogenic cells, this is the CI dimer (*17*). For the P_{RM} reporter, we found the value of $\beta_{protein}$ to be close to half the one measured in the lysogen, suggesting that the most abundant species in the reporter was the CI monomer. The fluctuation analysis (see below, **section 2.3.2**) led to a similar conclusion.

2.3.2 Estimating the fluorescence of a single CI molecule using the fluctuations of immunofluorescence intensity. Our method was inspired by the one developed by Rosenfeld *et al*. for counting fluorescent proteins in live cells (*16*). For a full derivation of our method, see (*18*). The principle is as follows: Given a cell with N copies of the protein of interest, if we assume that the proteins are distributed randomly inside the cell cytoplasm, the probability P(n_1, n_2 ,n_3 , … , n_m) of finding (n_1, n_2 , n_3 , … , n_m) molecules in the m voxels of the cell will be given by a multinomial distribution. The mean and variance of the multinomial distribution are linearly related, with a slope that depends on the probability p_i of finding a particle inside a voxel i. Then, if we assume that the image produced by a single fluorescent particle can be approximated by a 3D Gaussian Point Spread Function (PSF), the slope k of a plot of the variance versus mean of the pixel intensities inside each cell will be given by:

$$k \approx \frac{A}{8(\pi)^{3/2}\sigma_x\sigma_y\sigma_z}, \qquad (3)$$

where A is the integral of the PSF in 3D, and σ_i are the widths of the PSF in each dimension.

To calculate the mean and variance of the pixel intensities in individual cells, we first subtracted the background fluorescence (defined as the mode of the pixel intensities of non-cell pixels) from each image in an immunofluorescence *z*-stack. We then calculated the mean and variance of the pixel intensities in each cell at the best-focus image (the one with the highest variance in pixel intensities of the whole image). The variance versus mean data was then fitted to a line, using the *polyfit* function in MATLAB (**Fig. 2D** and **fig. S10B**). We converted the slope k to the total intensity of a single particle at its best focus using the relation:

$$I_{\text{spot}} = 4\pi\sqrt{2}\sigma_x\sigma_y k. \qquad (4)$$

In the lysogen, I_{spot} is expected to correspond to the intensity of a CI dimer (*17*). In the case of the P_{RM} reporter, we divided the curve into two sections, one for low and the other for high CI concentrations. The slope at high concentrations was approximately twice the slope observed at low CI concentrations, suggesting that, as expected, the most abundant species at low CI concentration is the monomer, whereas the most abundant species at high CI concentration is the dimer (**fig. S7**).

2.3.3 Estimating the number of CI proteins in a lysogen. To calculate the number of CI monomers in a lysogen, the total background-subtracted fluorescence inside lysogenic and non-lysogenic cells was divided by the estimated fluorescence of a single CI monomer. The value found in the negative samples (12 ± 2, mean ± SEM over 12 experiments) was subtracted from the number of CI monomers found in the lysogen sample. Estimates of the number of CI monomers in a lysogen obtained using spot quantification and fluctuation analysis were in good agreement (**Fig. 2D** and **fig. S4B**) and the estimates from IF-smFISH experiments were similar to the ones from immunofluorescence alone (**fig. S10C**). Our estimates were inside the range of values reported in the literature (**Fig 2D**, **table S2**).

2.3.4 Estimating CI concentration in the P_{RM} reporter system. CI concentration inside the cell was calculated as follows:

$$[\text{CI}] = \frac{\langle I \rangle}{\sqrt{2\pi}\sigma_z I_{\text{spot}} A_{\text{pix}} N_a}, \qquad (5)$$

where [CI] is the molar concentration of CI monomers inside the cell, $\langle I \rangle$ is the mean fluorescence intensity per pixel inside the cell, σ_z is the width of the PSF produced by a single protein molecule along the *z*-axis, I_{spot} is the total intensity produced by a single CI monomer (calculated in **section 2.3.2**), A_{pix} is the area of the image pixel, and N_A is Avogadro's number. We used $\sigma_z = 2.19 \cdot 10^{-7}$ m, which is the expected value for Alexa488 assuming that the PSF can be described by a 3D Gaussian function (*38*).

2.4 Measuring the gene copy number

2.4.1 Estimating the number of P_{RM} copies in individual cells. We used the *galK* locus, which is ~16 kb away from the lambda integration site (*att*B), as a proxy for the position of the P_{RM} promoter in a lysogen. Strain LSG03 was grown as described in **section 1.2**, and imaged as described in **section 1.7**. Fluorescent spots were recognized using Spatzcells, as described in **section 2.2**. The spot intensities calculated by Spatzcells were used to generate a spot intensity histogram. The histogram showed a single peak. The number of P_{RM} copies was then calculated by counting the number of fluorescent spots in each cell.

2.4.2 Identifying cell populations with a defined number of copies of the P_{RM} promoter. We first discarded cells without florescent foci (<5%, presumably due to loss of the TetR-YFP expression plasmid). Cells were then sorted according to length. In the gene-copy analysis, we ignored cells in percentiles <5 and >95, so as to exclude outlying spherical or filamentous cells. We found that short ("newborn") cells, spanning percentiles 5-20 in cell length, had an average of 2.1 ± 0.1 (mean ± SEM) gene copies per cell (**Fig. 3B**, N = 493), while long cells (about to divide), spanning percentiles 80-95, had an average of 4.0 ± 0.1 gene copies per cell (**Fig. 3B**, N = 493). These numbers were in good agreement with the expected number under our growth conditions (*26*), and these gates were therefore used in the subsequent analysis

2.4.3 Estimating the fraction of cells with 2 or 4 of copies of the P_{RM} promoter. Cells were sorted according to cell size, and cells in percentiles 0-5 and 95-100 were discarded. The fraction of cells containing 2 copies of the P_{RM} promoter was defined as:

$$\alpha = \frac{N_2}{N_2 + N_4}, \qquad (6)$$

where N_2 and N_4 are the number of cells with 2 and 4 fluorescent foci, respectively. We measured $\alpha = 0.61$ (N = 1202 cells).

2.5 mRNA quantification

2.5.1 Measuring the number of target mRNA in individual cells. mRNA copy numbers for each cell in negative and positive samples were estimated as previously described (*25*). Briefly, mRNA spots were first recognized using Spatzcells (**section 2.2**). Next, we generated peak height histograms for the spots from negative and positive samples (**fig. S8**). A threshold in peak height was used to discard spots in the positive sample that overlapped the spots from the negative sample. The remaining spots were used to generate a spot intensity histogram (**fig. S8**). The histogram was fitted to a multi-Gaussian function of the form:

$$f_{\mathrm{mRNA}}(I) = \sum_{i=1}^{3} \phi_i e^{-\frac{(I - i\beta_{mRNA})^2}{2i\gamma^2_{mRNA}}}, \qquad (7)$$

where ϕ_i is the amplitude of each Gaussian, β_{mRNA} and γ^2_{mRNA} are the mean and variance of the fluorescence intensity of a single mRNA molecule. ($2\beta_{mRNA}$, $2\beta_{mRNA}$) and ($3\gamma^2_{mRNA}$, $3\gamma^2_{mRNA}$) correspond to the mean and variance of the fluorescence intensities of spots containing 2 and 3 mRNA, respectively. The total number of mRNA from the target gene in each cell was then obtained by summing the intensities of all spots above the peak height threshold and dividing the total intensity by β_{mRNA}. Results from smFISH and IF-smFISH experiments were in good agreement for both lysogenic and P_{RM} reporter strains (compare **fig S8** and **fig. S10**, **D** and **E**). All fits were performed using the nonlinear least squares method (implemented using the *fit* function in MATLAB).

2.5.2 Estimating the transcriptional activity of a single gene copy. Cells were sorted according to length, and cells in percentiles 0-5 and 95-100 were discarded. We identified cells with 2 and 4 P_{RM} copies using the cell-length criteria described in **section 2.4**. The mean number of *cI* mRNA in long cells (8.56 ± 0.26, mean ± SEM for 497 cells) was close to double the one observed in short cells (4.59 ± 0.18, 497 cells). We then generated the mRNA copy-number histograms for long and short cells (**fig. S9**). Each histogram was then fitted independently to the prediction from a two-state model of transcription (*23, 39*). In this model, a promoter in the inactive (off) state can transition to the active (on) state with probabilistic rate k_{on}. In the active state, the promoter can produce mRNA with probabilistic rate k_{TX}. mRNA is degraded with probabilistic rate k_{d}. The promoter transitions back to the inactive state with probabilistic rate k_{off}. In the limit where $k_{\mathrm{off}} \gg k_{\mathrm{d}}$ and $k_{\mathrm{off}} \gg k_{\mathrm{on}}$, transcription occurs in short, rapid bursts, and the mRNA copy-number statistics can be described using a negative binomial distribution (*23, 39*):

$$P(m; r, p) = \binom{m + r - 1}{m} p^r (1 - p)^m, \qquad (8)$$

where m is the number of mRNA in the cell, r is the burst frequency (in units of bursts per mRNA lifetime), and p is the probability that the gene switches from the active to the inactive state prior to producing another mRNA (related to the burst size b through the relation $b = (1 - p)/p$). The negative binomial fits were in good agreement with the experimental distributions (**fig. S9A**). If each of the copies of the P_{RM} promoter is transcriptionally independent, then the mRNA copy-number distribution for long cells (with 4 copies of the P_{RM} promoter) should be given by the autoconvolution of the distribution for short cells (with 2 copies of the P_{RM} promoter), which would in turn be given by the autoconvolution of the distribution for a single P_{RM} copy (*13, 40*). Using the fact that the n-convolution of a negative binomial distribution is given by:

$$P(m; r, p)^{*n} = P(m; nr, p), \qquad (9)$$

we fitted the mRNA copy-number histogram of short cells to $P(m; 2r, p)$ and the one of long cells to $P(m; 4r, p)$. This, again, agreed well with the experimental data (**fig. S9B**). The parameters from the fit allowed us to obtain the expected mRNA copy-number distribution for a single copy of P_{RM}, $g = P(m; r, p)$. Finally, the autoconvolution of the mRNA histogram for short cells showed a good agreement with the measured histogram for long cells (**fig. S9C**), consistent with the gene copies having independent transcriptional activities. All the fits described in this section were performed using maximum likelihood estimation (see **section 3.2**). The parameter search was performed using the simulated annealing routine (*simulannealbnd*) of MATLAB.

2.5.3 Reconstructing the mRNA distribution of the whole cell population from the single-gene distribution. After obtaining the expected mRNA distribution g of a single P_{RM} promoter (**Section 2.6.2**) and the fraction of cells with 2 and 4 copies of the P_{RM} promoter (**section 2.5.3**), we reconstructed the mRNA copy-number histogram of the whole cell population (*13*):

$$P(m) = \alpha g^{*2} + (1-\alpha) g^{*4}, \qquad (10)$$

where α is fraction of cells containing 2 copies of the P_{RM} promoter. The reconstructed distribution showed good agreement with the experimental data (**Fig. 3A**).

3 Modeling P_{RM} regulation

3.1 Thermodynamic model.

3.1.1 Description of the model. To describe the mean P_{RM} regulatory curve, we implemented the equilibrium thermodynamic model described by Dodd *et al.* (*15*). In this model, each CI dimer binding site ($O_{R1\text{-}3}$ and $O_{L1\text{-}3}$) can be either occupied or unoccupied, allowing 64 unlooped binding configurations. Additionally, configurations having two adjacent sites occupied in both operators can create a DNA loop, allowing 9 looped configurations (**fig. S12A**). The probability of finding P_{RM} in configuration i is given by:

$$P_i\left(\left[\mathrm{CI}\right]\right) = \frac{e^{-\Delta G_i/RT}\left[\mathrm{CI}_2\right]^{n_i}}{\sum_i e^{-\Delta G_i/RT}\left[\mathrm{CI}_2\right]^{n_i}}, \quad (11)$$

where $[CI_2]$ is the concentration of free (not DNA-bound) CI dimers in the cell, n_i is the number of CI dimers bound to the O_R/O_L operators in the configuration i, and ΔG_i is the free energy of the configuration, given by:

$$\Delta G_i = \boldsymbol{\delta}_i \cdot \mathbf{\Delta G}, \quad (12)$$

where $\mathbf{\Delta G}$ is a vector with all possible free energy contributions and $\boldsymbol{\delta}_i$ is a binary vector selecting the free energy contributions present in the configuration i. $\mathbf{\Delta G}$ is defined as:

$$\mathbf{\Delta G} = \left[\Delta G_{O_{R1}}, \Delta G_{O_{R2}}, \Delta G_{O_{R3}}, \Delta G_{O_{L1}}, \Delta G_{O_{L2}}, \Delta G_{O_{L3}}, \Delta G_{\mathrm{Adj}}^{O_R}, \Delta G_{\mathrm{Adj}}^{O_L}, \Delta G_{\mathrm{Oct}}, \Delta G_{\mathrm{Tet}}\right]. \quad (13)$$

$\Delta G_{O_{Rj}}$ and $\Delta G_{O_{Lj}}$ are the free energies for binding of a CI dimer to the corresponding operator sites. $\Delta G_{\mathrm{Adj}}^{O_R}$ and $\Delta G_{\mathrm{Adj}}^{O_L}$ are the free energies of interaction between CI dimers located on adjacent binding sites (only one of these terms is allowed per operator). ΔG_{Oct} is the free energy of interaction between adjacent CI dimers from O_L and O_R to create a CI octamer, present in all looped configurations. ΔG_{Tet} is the free energy of interaction between CI dimers located in sites O_{L3} and O_{R3} to create a CI tetramer, present only in the looped configuration where all sites are occupied. The relationship between the total concentration of CI monomers in the cell [CI] and the concentration of free CI dimers is given by:

$$\left[\mathrm{CI}\right] = 2\left[\mathrm{CI}_2\right] + \sqrt{\frac{\left[\mathrm{CI}_2\right]}{K_{\mathrm{Dim}}}} + 2K_{\mathrm{NS}}\left[\mathrm{CI}_2\right]\left[\mathrm{NS}\right], \quad (14)$$

where K_{Dim} is the CI dimerization constant, K_{NS} is the equilibrium constant for non-specific binding of CI dimers to DNA, and [NS] is the concentration of non-specific binding sites in the cell. The promoter configurations were grouped into four states, according to their transcriptional activity: basal, unlooped activated, looped activated and repressed (**fig. S12A** (*15*)). The mean mRNA expression level for the P_{RM} promoter in a cell with a particular CI concentration is given by:

$$M\left(\left[\mathrm{CI}\right]\right) = (4-2\alpha)\sum_{i=\{\mathrm{B,U,L,R}\}} M_i P_i. \qquad (15)$$

where α is the fraction of cells in the population with 2 copies of the P_{RM} promoter, estimated using the *galK* reporter (**section 2.4.3**), and the factor $(4 - 2\alpha)$ is the mean number of P_{RM} copies per cell. M_B, M_U, M_L and M_R are, respectively, the mean mRNA expression levels for a single P_{RM} promoter in the basal, unlooped activated, looped activated and repressed promoter states, while $P_i([CI])$ is the probability of the promoter state *j*, given by:

$$P_j\left(\left[CI\right]\right) = \sum_{i\in j} P_i\left(\left[CI\right]\right). \quad (16)$$

3.1.2 Fitting procedure. Cells of the P_{RM} reporter were sorted according to length, and cells in percentiles 0-5 and 95-100 were discarded. The total number of *lacZ* mRNA in each cell was measured as described in **section 2.6.1**. CI protein concentration in each cell was measured as described in **section 2.3.4**. The experimental data was fitted to the model in **section 3.1.1** by minimizing the root-mean-square deviation between the data and the model. For the fit, the parameters K_{NS}, ΔG_{Tet}, ΔG_{Oct}, M_B, M_U and M_R were allowed to vary. M_L was set to $0.75M_U$, based on previous measurements (*15*). All the other parameter values were taken to be equal to the ones used by Dodd *et al*. (*15*) (**table S5**). We note that previous studies reported that the repressed state of the P_{RM} promoter has negligible transcriptional activity (*4, 5, 15, 28*). We repeated the fitting procedure while imposing $M_R = 0$. This slightly decreased the quality of the fit (from $R^2 = 0.981$ to $R^2 = 0.970$, **fig. S13**). The parameter search was performed using the simulated annealing routine (*simulannealbnd*) of MATLAB.

3.2 Stochastic kinetic model.

3.2.1 Description of the model: The model is described schematically in **Fig. 4E**. Each of the four promoter states introduced in **section 3.1** is described using a two-state model of transcription (**section 2.6**). The linear topology of transitions between promoter states (basal ↔ unlooped activated ↔ looped activated ↔ repressed) is supported by the topology of full thermodynamic model, when only the most probable configurations are considered (**fig. S12**, **C** – **D**). For simplicity, transitions between different promoter states were only allowed between the "inactive" states of each promoter state (**Fig. 4E**). We first solved the model in the limit where the transition between different promoter states

is very fast compared to mRNA lifetime (**Fig. 4G, right**; see **section 3.4** below for the more general case). In this limit, the expected *lacZ* copy-number distribution for a single P_{RM} promoter in a cell with CI concentration [CI] is given by:

$$g\left(m;[\mathrm{CI}]\right)=P\left(m;\rho_B,p_B\right)*P\left(m;\rho_U,p_U\right)*P\left(m;\rho_L,p_L\right)*P\left(m;\rho_R,p_R\right), \qquad (17)$$

where $P\left(m;\rho_j([\mathrm{CI}]),p_j\right)$ is a negative binomial distribution (**section 2.5.2**) representing the contribution of the promoter state *j* to the mRNA copy-number histogram of a single P_{RM} promoter, the parameter p_j is related to the burst size b_j of the promoter state *j* via $b_j = (1 - p_j)/p_j$, and the parameter ρ_j is given by:

$$\rho_j = P_j\left([\mathrm{CI}]\right)r_j, \qquad (18)$$

where P_j([CI]) the probability of the promoter state *j* from the thermodynamic model, and r_j is the burst frequency for the promoter state *j*. The mRNA copy-number distribution for all cells in the population was then calculated as:

$$P\left(m;[\mathrm{CI}]\right)=\alpha g\left(m;[\mathrm{CI}]\right)^{*2}+\left(1-\alpha\right)g\left(m;[\mathrm{CI}]\right)^{*4}, \qquad (19)$$

where α is the fraction of cells in the population with 2 copies of the P_{RM} promoter (**section 2.4.3**). The mean expression level of the promoter state *j* in the thermodynamic model is related to the stochastic kinetics of transcription through the relation:

$$M_j = r_j b_j. \qquad (20)$$

As a result, the stochastic model uses 4 independent parameters describing the kinetics of the promoter states (r_i and b_i, i = 1 to 4, with 4 constraints via M_j, j = 1 to 4), in addition to the ones used in the thermodynamic model.

3.2.2 *Maximum likelihood estimation*. Cells of the P_{RM} reporter were sorted according to protein concentration and separated into *N* bins of *M* cells each. We then calculated the likelihood that our data was described by the model, using a likelihood function:

$$L\left(\hat{\theta}\right)=\prod_{i=1}^{N}\prod_{j=1}^{M}P\left(m_j,[\mathrm{CI}]_i,\hat{\theta}\right), \quad (21)$$

where $P(m_j,[\mathrm{CI}]_i,\hat{\theta})$ is the probability predicted by the stochastic model, with a parameter set $\hat{\theta}$, of observing a cell with m_j mRNA and a CI concentration $[\mathrm{CI}]_i$. For each bin *i*, we calculated $[\mathrm{CI}]_i$ as the average CI concentration of the cells inside the bin. To find the best set of parameters $\hat{\theta}$ that reproduce our experimental observations m_j for all bins, we took the natural logarithm of the likelihood function and searched for the

parameter set that maximized the log-likelihood that our data was predicted by the stochastic model (*41*):

$$\hat{\theta}_{\text{fit}} = \arg\max_{\hat{\theta}} \log\left(L\left(\hat{\theta}\right)\right) = \arg\max_{\hat{\theta}} \sum_{i=1}^{N}\sum_{j=1}^{M} \log\left(P\left(m_j;[\text{CI}]_i,\hat{\theta}\right)\right), \qquad (22)$$

where $\hat{\theta}_{\text{fit}}$ is the maximum likelihood estimate of the parameters of our stochastic model, given our experimental data. For fitting, we used 100 cells per bin, and each bin had an overlap of 50 cells with each adjacent bin. Our estimates were robust to the specific number of cells per bin used for the fit. The parameter search was performed using the simulated annealing routine (*simulannealbnd*) of MATLAB. The parameters obtained from the fit are shown in **fig. S15C** and **table S6**.

3.3 Genetic controls for the pure promoter states.

To obtain an independent validation of the parameters obtained from the stochastic model, we sought to directly measure the transcriptional parameters of the different promoter activity states. To estimate the activity of the basal state, we used a P_{RM} reporter strain in the absence of CI expression (AP327, **table S1**). To estimate the activity of the repressed and of the unlooped activated state, we used, respectively, the P_{RM} reporter with and without the O_{L} operator (AP365 and AP326, **table S1**), expressing high levels of CI. Cells for the three genetic controls were grown according to **section 1.2** and labeled using IF-smFISH (**section 1.6**). mRNA and protein concentrations were measured as described in **section 2**. For the case of strains AP326 and AP365, cells were sorted according to CI concentration, and the mean mRNA per cell as a function of CI was calculated using a moving average. Only cells inside a plateau in mRNA levels were used (**Fig. S15A**, top). Next, for each of the samples described above, we estimated the transcriptional activity of a single copy of the P_{RM} promoter as described in **section 2.6** (**Fig. S15A**, bottom). A comparison of the transcriptional parameters estimated from the three genetic controls with the fit to the stochastic model is shown in **fig. S15C** and **table S5**.

3.4 Solving the stochastic model for different switching rates between promoter activity states.

3.4.1 Description of the general model. In **section 3.2.1**, we solved the stochastic model in the limit where the transition rates between different promoter states were faster than the mRNA lifetime. We sought to test this assumption by solving the stochastic model depicted in **Fig. 4E** for a wider range of switching rates. To achieve this, we first formulated the Chemical Master Equation (CME) for the activity of a single P_{RM} promoter, which is an infinite set of ordinary differential equations that describe the time

evolution of the probabilities $P_{s,m}$ of finding the promoter in the transcriptional state s, in a cell containing m mRNA produced from the P_{RM} promoter (*41*, *42*). The CME can be written in matrix form:

$$\dot{\mathbf{P}} = \mathbf{M}\mathbf{P}$$

$$\frac{d}{dt}\begin{bmatrix}\mathbf{P}_0\\ \mathbf{P}_1\\ \mathbf{P}_0\\ \vdots\end{bmatrix} = \begin{bmatrix}\mathbf{A}-\mathbf{T} & \mathbf{D} & 0 & \cdots\\ \mathbf{T} & \mathbf{A}-\mathbf{T}-\mathbf{D} & 2\mathbf{D} & \cdots\\ 0 & \mathbf{T} & \mathbf{A}-\mathbf{T}-2\mathbf{D} & \cdots\\ \vdots & \vdots & \vdots & \ddots\end{bmatrix}\begin{bmatrix}\mathbf{P}_0\\ \mathbf{P}_1\\ \mathbf{P}_0\\ \vdots\end{bmatrix}, \qquad (23)$$

here, $\mathbf{P}_m$ is a vector with all the states of the system having m mRNA, given by:

$$\mathbf{P}_m = \left[P_{\mathrm{B_{off}},m}, P_{\mathrm{B_{on}},m}, P_{\mathrm{U_{off}},m}, P_{\mathrm{U_{on}},m}, P_{\mathrm{L_{off}},m}, P_{\mathrm{L_{on}},m}, P_{\mathrm{R_{off}},m}, P_{\mathrm{R_{on}},m}\right]^T, \quad (24)$$

where the indices (B, U, L, R) refer to the basal, unlooped activated, looped activated and repressed promoter states, and (on, off) refer to the inactive and active states describing each promoter state (**Fig. 4E**). **D**, **T**, and **A** are 8 × 8 submatrices describing degradation, transcription, and switching between states, of the form:

$$\mathbf{D} = k_{\mathrm{d}}\mathbf{I}_8,$$

$$\mathbf{T} = \begin{bmatrix}\mathbf{T_1} & 0 & 0 & 0\\ 0 & \mathbf{T}_2 & 0 & 0\\ 0 & 0 & \mathbf{T}_3 & 0\\ 0 & 0 & 0 & \mathbf{T}_4\end{bmatrix}, \qquad (25)$$

$$\mathbf{A} = \begin{bmatrix}\mathbf{A}_1-\mathbf{S}_1 & \mathbf{S}_2 & 0 & 0\\ \mathbf{S}_1 & \mathbf{A}_2-\mathbf{S}_2-\mathbf{S}_3 & \mathbf{S}_4 & 0\\ 0 & \mathbf{S}_3 & \mathbf{A}_3-\mathbf{S}_4-\mathbf{S}_5 & \mathbf{S}_6\\ 0 & 0 & \mathbf{S}_5 & \mathbf{A}_4-\mathbf{S}_6\end{bmatrix},$$

where k_{d} is the mRNA degradation rate (0.5 min^{-1} for *lacZ* (*29*)), while $\mathbf{T}_j$, $\mathbf{A}_j$ and $\mathbf{S}_j$ are 2 × 2 submatrices of the form:

$$\mathbf{T}_j = \begin{bmatrix}0 & 0\\ 0 & k_{\mathrm{TX}}^j\end{bmatrix},$$

$$\mathbf{A}_j = \begin{bmatrix}-k_{\mathrm{on}}^j & k_{\mathrm{off}}^j\\ k_{\mathrm{on}}^j & -k_{\mathrm{off}}^j\end{bmatrix}, \qquad (26)$$

$$\mathbf{S}_j = \begin{bmatrix}k_j & 0\\ 0 & 0\end{bmatrix},$$

where k_{TX}^{j} is the transcription rate in the active state of the promoter state j, k_{on}^{j} and k_{off}^{j} are, respectively, the rates for turning "on" and "off" the P_{RM} promoter in promoter state j, and k_j are the transition rates between the inactive states of different promoter states (see **Fig. 4E**).

To obtain the parameters for the model, we first assumed that each promoter state can be described using the rapid bursts approximation for the two-state model (*23, 39*). Under this approximation, we expressed the parameters describing the kinetics for each promoter state j in terms of the burst frequency r_j and burst size b_j obtained using the stochastic fit:

$$\begin{aligned} k_{\mathrm{off}}^{j} &= \omega k_{\mathrm{d}}, \\ k_{\mathrm{on}}^{j} &= r_j k_{\mathrm{d}}, \\ k_{\mathrm{TX}}^{j} &= k_{\mathrm{off}}^{j} b_j, \end{aligned} \qquad (27)$$

where ω is a scalar, and r_j and b_j are respectively the burst frequency and burst size of a single P_{RM} promoter in the promoter state j, obtained from the stochastic fit in **section 3.2.1**. To comply with the rapid burst limit, we used ω = 1000 (testing lower values indicated that ω above 10 still allows us to obtain a good fit between the model and experiment. This corresponds to k_{TX}~1 sec^{-1}, consistent with reported values for the rate of transcription initiation in *E. coli* (*43*)). The transition rates between different promoter states satisfy the following relations:

$$\begin{aligned} k_2 P_{\mathrm{B}}\left([\mathrm{CI}]\right) &= k_1 P_{\mathrm{U}}\left([\mathrm{CI}]\right), \\ k_4 P_{\mathrm{U}}\left([\mathrm{CI}]\right) &= k_3 P_{\mathrm{L}}\left([\mathrm{CI}]\right), \\ k_6 P_{\mathrm{L}}\left([\mathrm{CI}]\right) &= k_5 P_{\mathrm{R}}\left([\mathrm{CI}]\right), \end{aligned} \qquad (28)$$

where $P_j([\mathrm{CI}])$ is the probability of observing the configuration group j at the CI concentration [CI]. Next, we set $k_1 = k_2 = k_3 = S$, where S is the switching rate between configuration groups used in the calculation (see below).

3.4.2 *Solving the Chemical Master Equation for a defined switching rate*. We solved the model described above using the Finite State Projection algorithm (FSP, (*42*)). In brief, FSP solves the CME numerically by truncating the transition matrix **M** into a finite matrix **M**'. The resulting finite set of ordinary differential equations, $\dot{\mathbf{P}}' = \mathbf{M}'\mathbf{P}'$, can then be solved using standard numerical techniques. We obtained the steady state solution of the system by solving $\mathbf{0} = \mathbf{M}'\mathbf{P}'$ using the routine *mldivide* in MATLAB. For the calculation, we truncated **M** to $m \leq 100$. The steady state mRNA copy-number histogram for a single P_{RM} copy was then calculated summing over all the states having the same number of mRNA. The mRNA copy-number histogram for the whole population for a particular switching rate S, $P(m;[\mathrm{CI}]_i, S, \hat{\theta})$ was calculated as described in **section 3.2**.

We solved the CME for 100 switching rates S_j (j = 1, 2, …, 100) in the interval 1×10^{-6} $s^{-1} < S_j < 1\times10^{6}$ s^{-1} (**Fig. 4G**). Cells of the P_{RM} reporter were sorted according to protein concentration and separated into N bins of M cells each. The CI concentration of bin i, $[CI]_i$, was calculated as the mean concentration of the cells in the bin. We used FSP to solve the stochastic model for every pair ($[CI]_i$, S_j}). We then calculated the log-likelihood that the experimental data is explained by the model for each switching rate S_j:

$$L_j = \log\left(L\left(S_j, \hat{\theta}_{\text{fit}}\right)\right) = \sum_{i=1}^{N}\sum_{k=1}^{M}\log\left(P\left(m_k; [\text{CI}]_i, S_j, \hat{\theta}_{\text{fit}}\right)\right), \qquad (29)$$

where $\hat{\theta}_{\text{fit}}$ is the parameter set for the stochastic model obtained in **section 3.2.2**, and m_k are the number of mRNA in the cells of bin i. To display the results, the log-likelihood was scaled to the interval [0,1] using the following relation:

$$L'_j = \frac{L_j - L_{\min(j)}}{L_{\max(j)} - L_{\min(j)}}, \qquad (30)$$

where $L_{\min(j)}$ and $L_{\max(j)}$ are, respectively, the log-likelihood of the model at the slowest and fastest switching rates. The resulting curve is shown in **Fig. 4G**.

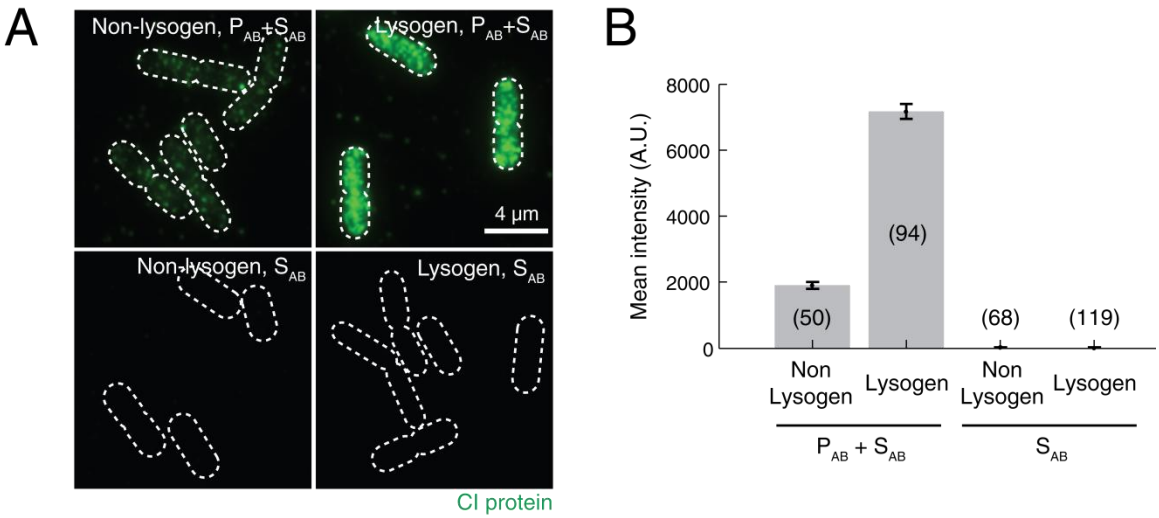

Fig. S1 Fluorescence signal in negative samples corresponds to non-specific binding of primary antibodies.

(A) Immunofluorescence images of non-lysogenic (MG1655) and lysogenic (MG1655 λ_{831}) cells treated with both unwashed anti-CI primary (P_{AB}) and secondary (S_{AB}) antibodies (top) or with secondary antibodies only (bottom). Dashed lines are cell contours, obtained from the phase contrast channel. (**B**) The mean pixel intensity above the background for the samples shown in panel A. Error bars are SEM over the number of cells indicated in parenthesis.

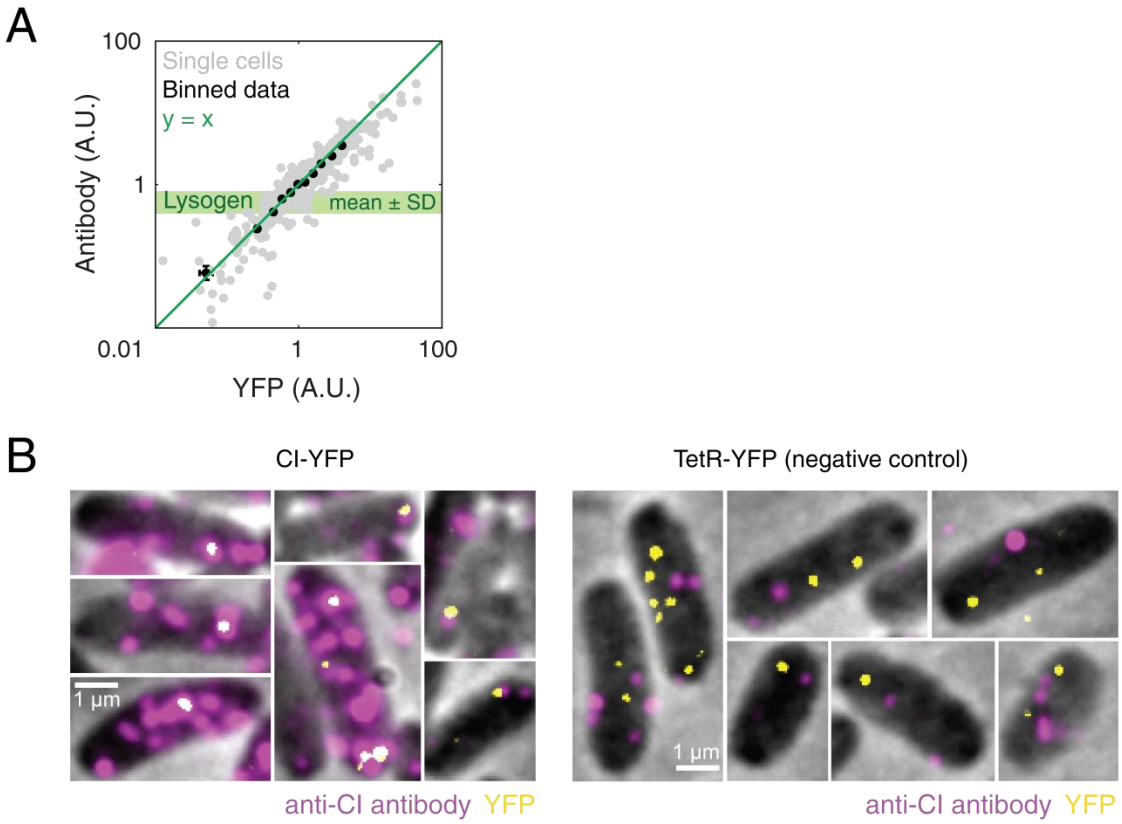

Fig. S2 Antibody labeling of CI-YFP fusion.

(**A**) Cells expressing different levels of CI-YFP (strain DH5αZ1(pZS21-*cIyfp*)) were grown, labeled using anti-CI antibodies, and imaged as described in **sections 1.2**, **1.3** and **1.7**. The CI immunofluorescence signal and YFP fluorescence were found to be linear over several orders of magnitude (N = 426 cells, R^2 = 0.84; error bars indicate SEM). The green shaded area indicates the immunofluorescence signal from lysogens (NK7049 λ_{WT} mean ± SD from 166 cells). (**B**) Single-molecule imaging of YFP and anti-CI antibodies. Low level of CI-YFP expression was induced as described in **section 1.2**, and the cells were labeled using anti-CI antibodies and Alexa647 secondary antibodies. Cells were then imaged as described in **section 1.7**. The majority of YFP molecules (40/55, yellow) were colocalized with an antibody signal (magenta). In a control sample expressing TetR-YFP (strain DH5αZ1(pZS21-*tetRyfp*)), no significant colocalization was observed The images above were smoothed using a 3x3 Gaussian kernel for visualization purposes, but the localization analysis was performed on the original raw images.

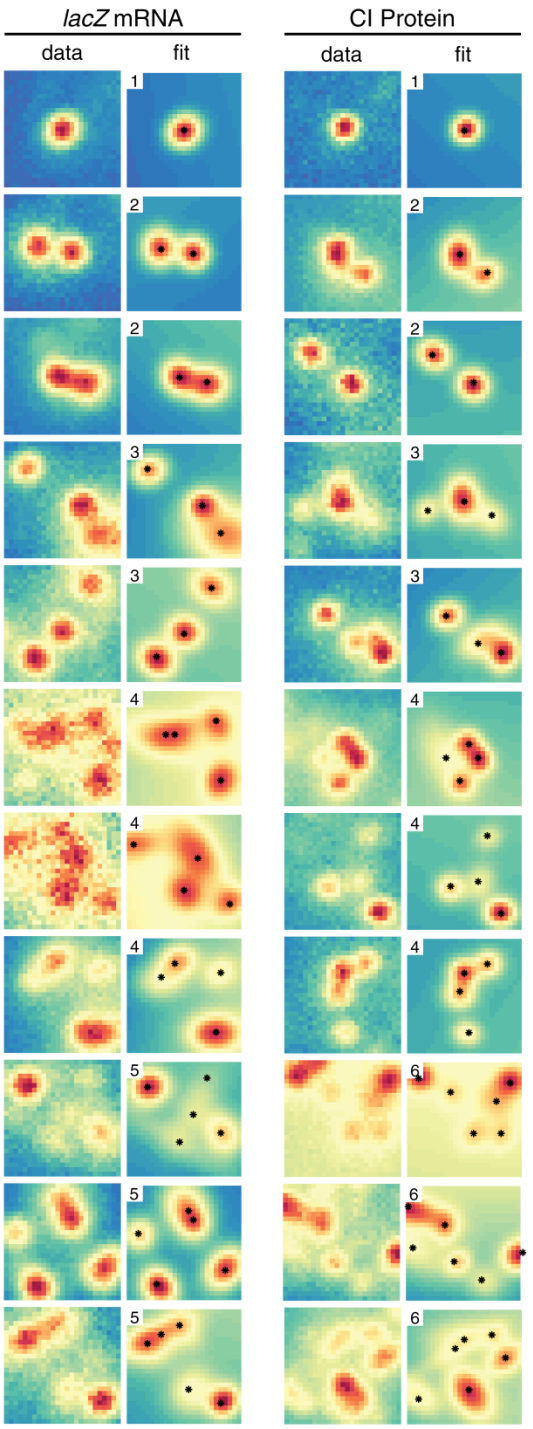

Fig. S3 Automated spot recognition.

Representative images of mRNA (left) and protein (right) spots next to the reconstructed images obtained from the multi-Gaussian fit performed using Spatzcells (*25*) (see **section 2.2**). The number of Gaussians used within each fitting region is shown in the upper left corner of each reconstructed image. The peaks of the fitted Gaussians are shown as black markers. The size of each region is 1.3 µm x 1.3 µm.

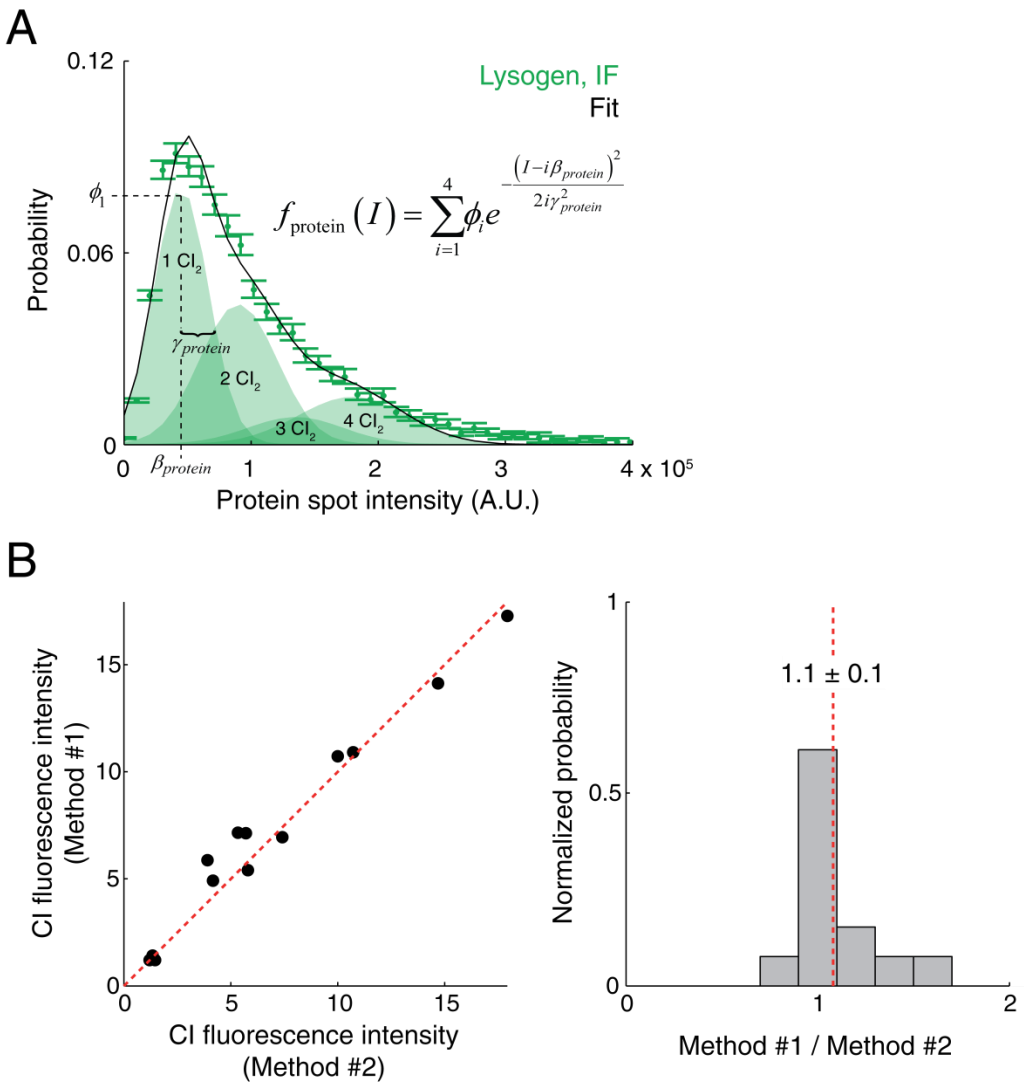

Fig. S4 Protein spot quantification and comparison with the fluctuation analysis.

(**A**) Estimating the fluorescence of single protein particles in a lysogen (NK7049 λ_{WT}) using spot quantification. Fluorescent spots in immunofluorescence (IF) images were detected using Spatzcells (*25*). Shown is the protein spot intensity histogram (N = 8810) for a representative sample (green markers, error bars are SEM for each bin). The histogram was fitted to a sum of Gaussian functions (black), corresponding to the expected fluorescence of spots containing 1 to 4 CI dimers (shaded green areas). The fluorescence of a CI dimer was estimated from the mean of the lowest-intensity Gaussian in the fitting function. (**B**) Comparison between the two protein quantification methods. (Left) The estimated fluorescence per CI dimer. Each data point represents the result of one independent experiment (99 to 883 cells, 1211 to 20759 spots per experiment). The samples include two lysogenic strains (MG1655 λ_{831} and NK7049 λ_{WT}) grown in two different media (LB and M9 + casamino acids + glucose (Teknova)). The dashed line is Y = X (R^2 = 0.97). (Right) The distribution of ratios between the estimates from the two methods. Also shown is the mean ± SD of this ratio.

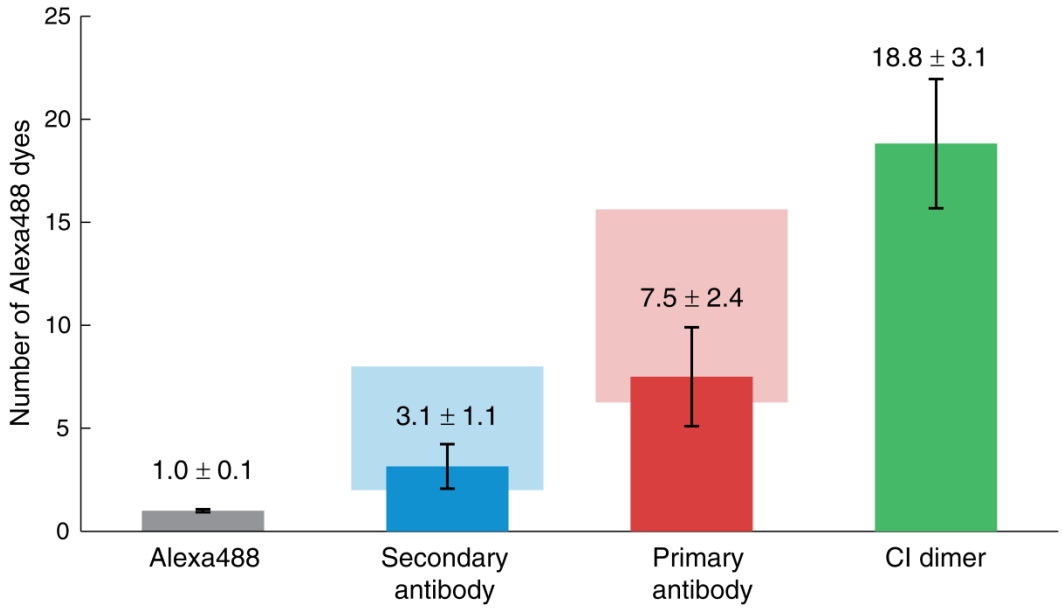

Fig. S5 The stoichiometry of protein labeling.

We used TIRF microscopy (see **section 1.7**) to measure the fluorescence of individual Alexa488 dyes (gray), secondary antibodies labeled with Alexa488 (blue), anti-CI primary antibodies labeled with Alexa488 secondary antibodies (red, measured in non-lysogenic cells) and CI dimers labelled with primary anti-CI antibodies and Alexa488 secondary antibodies (green, measured in lysogenic cells, NK7049 λ_{WT}). As an additional way of estimating some of these values, we measured the ratio in fluorescence between the secondary antibodies, primary antibodies and CI dimers in images of non-lysogenic (NK7049) and lysogenic cells (NK7049 λ_{WT}), analyzed using both the spot quantification and fluctuation methods (**section 2.3**). The results obtained from the different measurements were normalized by the intensity of the primary antibody and then averaged. The error bars represent the combined standard error from both measurements. The blue shaded area is the expected range of fluorescent dyes per secondary antibody (2-8, from the manufacturer) and the red shaded area is the expected range of fluorescent dyes per primary antibody (1-2 secondary antibodies per primary antibody, from the manufacturer).

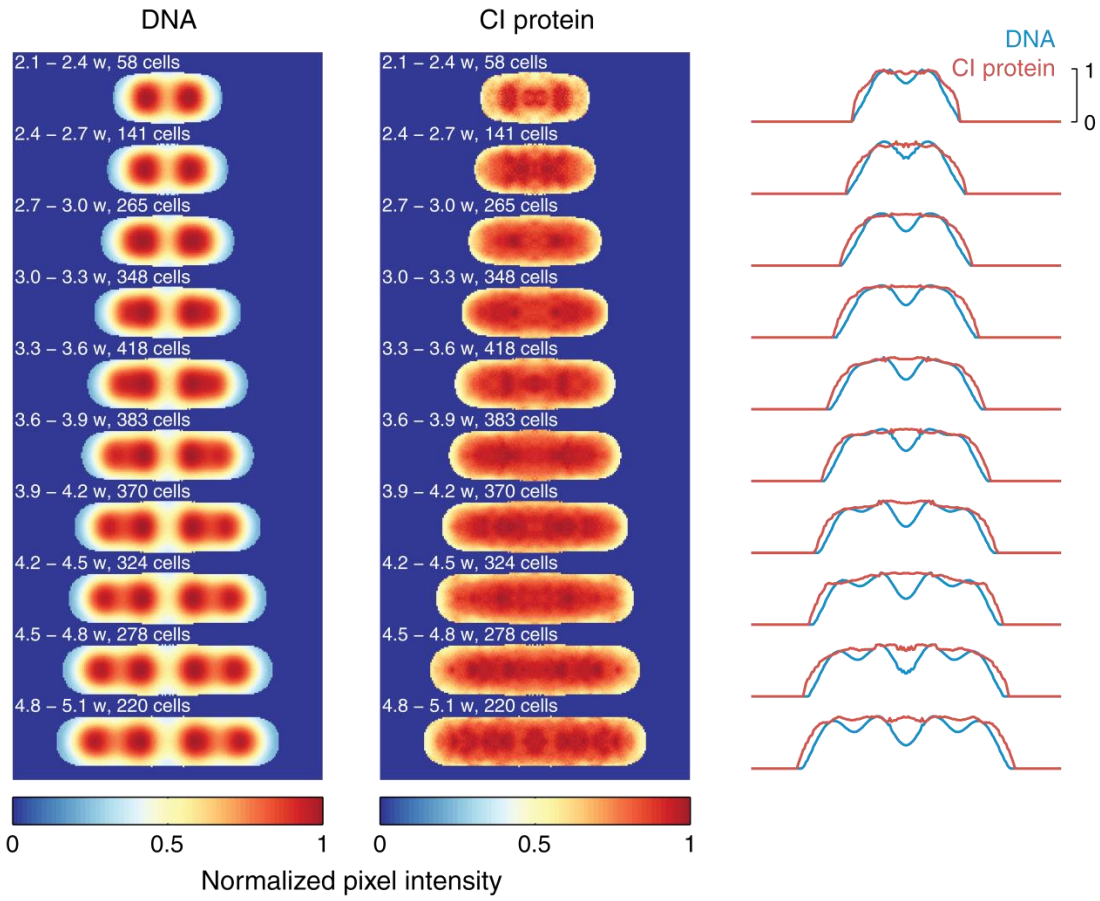

Fig. S6 The spatial distribution of CI proteins in the cell.

Fluorescent images of P_{RM} reporter (AP365) cells in the DAPI (DNA) and Alexa488 (CI protein) channels were binned based on cell length. All cells within a bin were then aligned, and the fluorescent intensity in each XY position averaged to generate a heatmap, following the method of (*44*). The corresponding one-dimensional intensity profiles are shown on the right. For each bin, the range of cell lengths (in units of cell width) is shown, along the number of cells averaged.

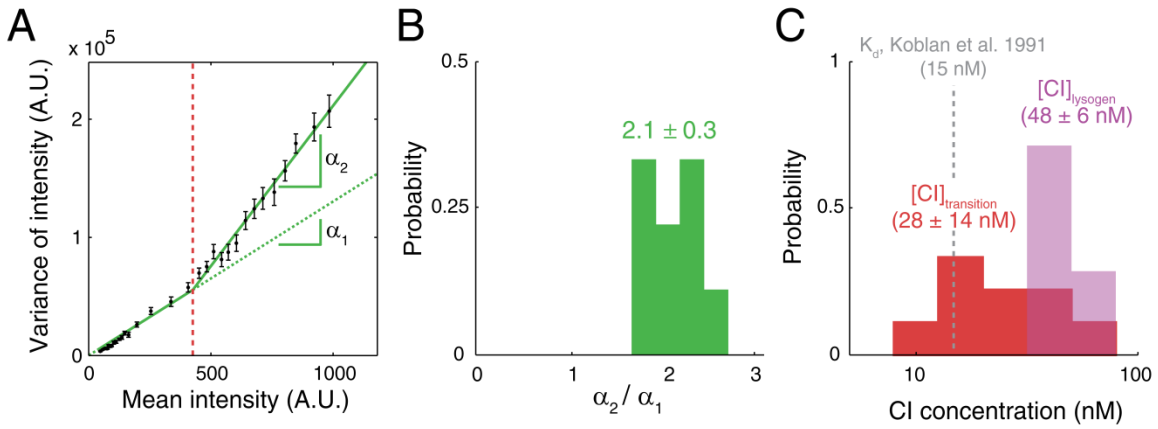

Fig. S7 Identifying CI monomers and dimers in the cell.

(**A**) A representative plot of the variance versus mean of pixel intensity in the CI antibody channel (P_{RM} reporter, AP365, N = 693 cells). The data was averaged over discrete bins of fluorescence intensity (black, mean ± SEM from 20 cells each), and then fitted to a piecewise linear model (green line). The vertical red line indicates the transition point between the two linear regimes. α_1 and α_2 are the slopes of the two green lines. (**B**) The ratio between the two slopes in the piecewise linear fit, from 9 independent experiments. The mean ± SD is also shown. (**C**) The CI monomer concentration corresponding to the transition between CI species. The pixel intensity at the intersection of the two linear regimes (panel A) was converted to protein concentration using the procedure described in **section 2.3.4** (red, data from 9 experiments). Also shown are the CI dimerization constant reported in the literature (gray, (*17*)) and the measured CI concentration in lysogenic cells (magenta, data from 6 experiments, numbers are the mean ± SD).

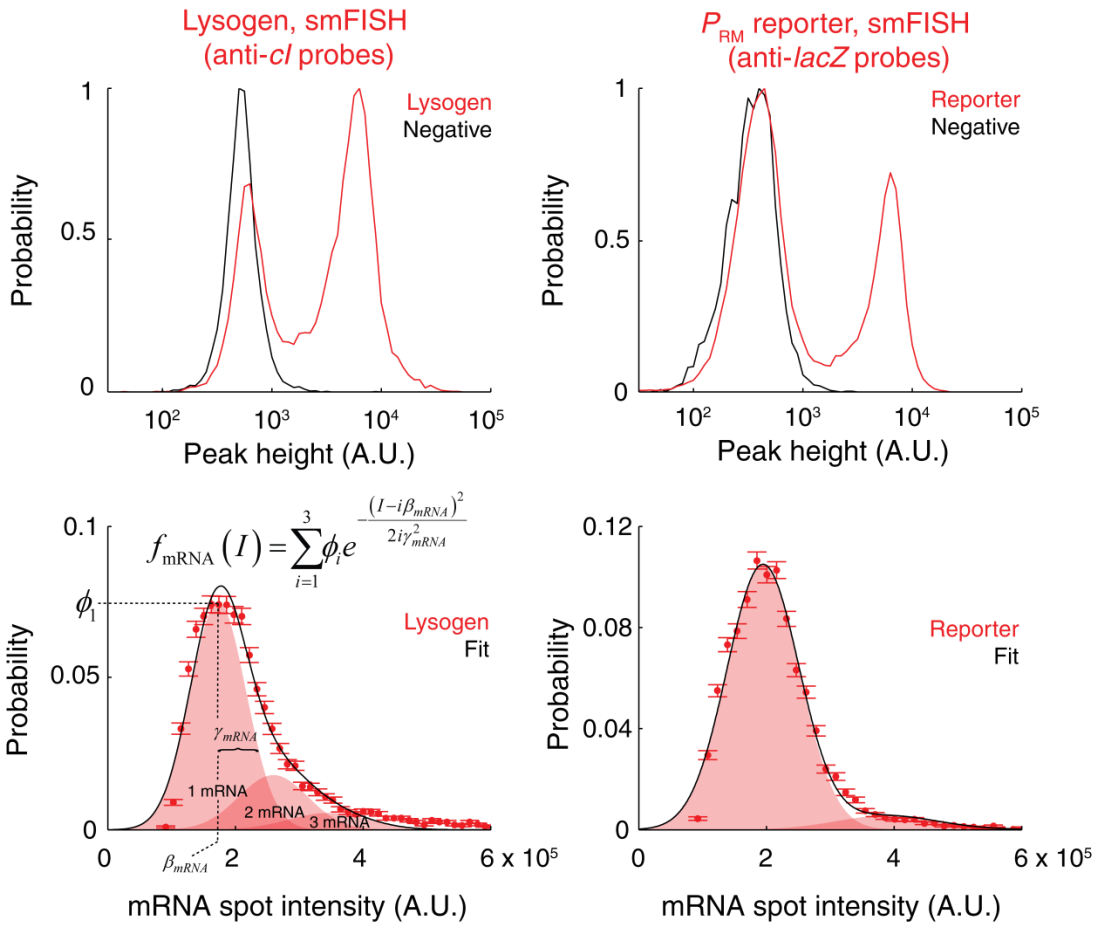

Fig. S8 Measuring the number of cI and lacZ mRNA in individual cells using smFISH.

Spots were quantified using Spatzcells (*25*). (Top) Representative peak height histograms of smFISH spots from lysogen (left, red, NK7049 λ_{WT}, N = 19693) and P_{RM} reporter cells (right, red, AP327, N = 34944), compared to negative samples lacking the target mRNA (black, NK7049, N = 6983 and 4213, respectively). The positive samples showed two well-separated peaks, one corresponding to non-specific binding of probes (found also in the negative sample) and the other to bona fide spots, present only in the positive sample. Spots in the positive sample due to the non-specific binding of probes were discarded and the remaining spots used to generate spot intensity histograms. (Bottom) mRNA spot intensity histograms of the positive samples shown above (lysogen, N = 9624; P_{RM} reporter, N = 9456). The mRNA spot intensity histograms (red markers, error bars are mean ± SEM for each bin) were fitted to a sum of multiple Gaussian functions (black line), corresponding to the expected fluorescence of spots containing 1 to 3 mRNAs (shaded red areas). The mean of the lowest-intensity Gaussian was used to estimate the fluorescence intensity of a single target mRNA (*25*).

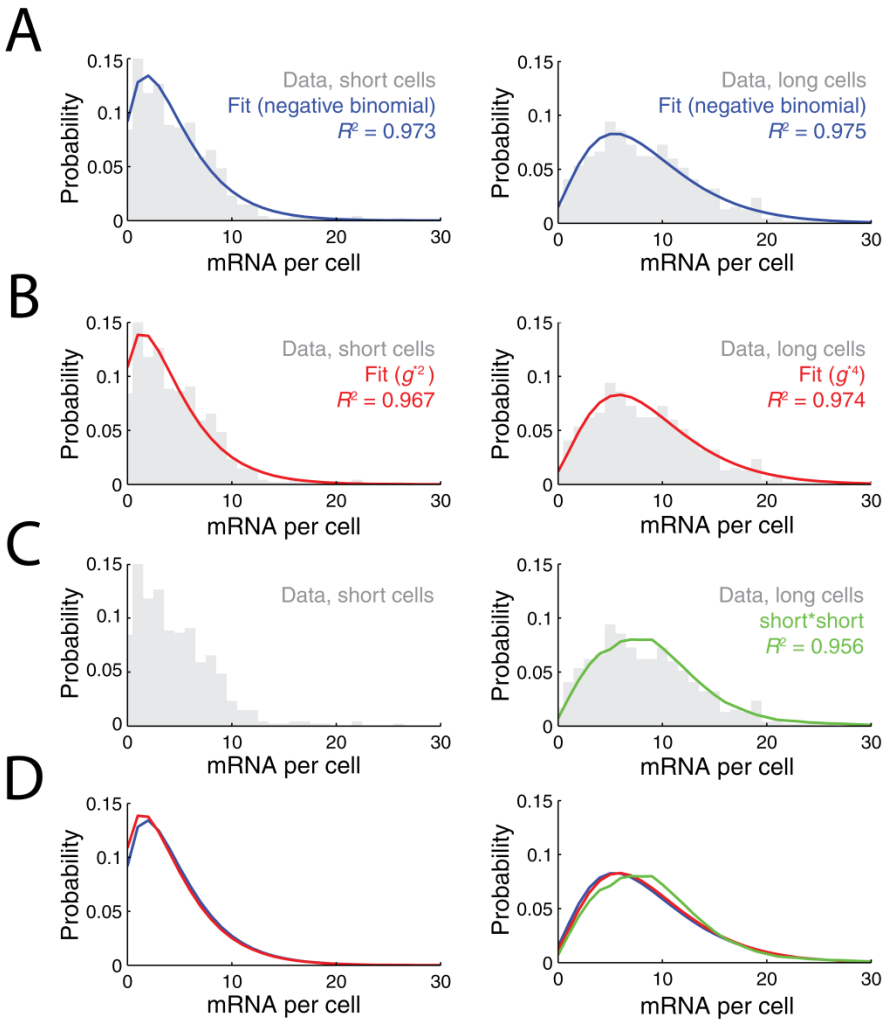

Fig. S9 Different copies of the PRM promoter are transcriptionally independent.

(**A**) *cI* mRNA copy-number histograms (gray) for short (left, N = 447, percentiles 5 to 15 in cell length) and long (right, N = 497, percentiles 80 to 95 in cell length) lysogenic cells (NK7049 λ_{WT}) were fitted to independent negative binomial distributions (blue). (**B**) The histograms of short (left, gray) and long (right, gray) cells were fitted simultaneously to $g^{*2} = P(m; 2r, p)$ and $g^{*4} = P(m; 4r, p)$ (red), respectively, where $P(m; r, p)$ is a negative binomial distribution describing the *cI* mRNA copy-number statistics of a single copy of the P_{RM} promoter, g. (**C**) The histogram of the short cells (gray, left) was autoconvolved (green) and overlaid with the histogram of long cells (gray, right). (**D**) Overlay of the curves shown in panels A to C.

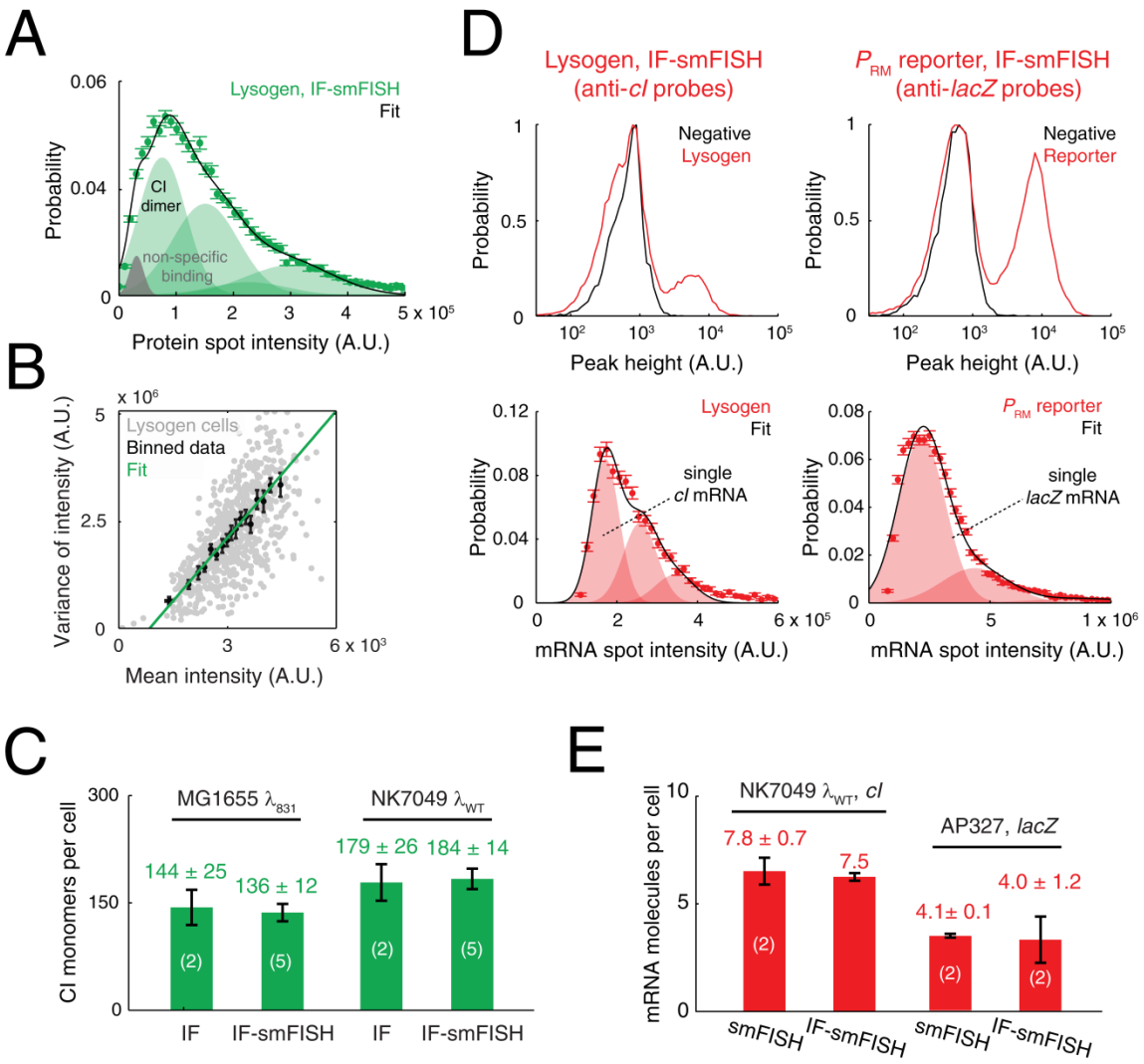

Fig. S10: Combined IF-smFISH protocol yields similar results to the separate protocols.

(**A**) A representative protein spot intensity histogram of lysogenic (NK7049 λ_{WT}) cells labeled using IF-smFISH (green markers, error bars are SEM for each bin, N = 17028). As in the case of IF alone (**fig. S4A**), the histogram is well described by a multi-Gaussian function (black) corresponding to the expected fluorescence of spots containing 1 to 4 CI dimers (shaded green areas). The contribution from non-specific binding, obtained from an independent fit to the negative sample, is shown in gray. (**B**) A representative plot of the variance versus mean for the pixel intensity of lysogenic cells (NK7049 λ_{WT}, gray, N = 706) labeled using IF-smFISH. Shown also is the average over discrete bins of fluorescence intensity (black, mean ± SEM). The data was fitted to a line whose slope was used to calculate the fluorescence of a single labeled CI dimer. (**C**) Estimated number of CI monomers per lysogen obtained from IF and IF-smFISH experiments, for two lysogenic strains. For each experiment, the number of CI proteins in each cell was calculated using spot quantification and fluctuation analysis, and the results averaged.

Error bars are mean ± SEM over the number of experiments shown in parenthesis. (**D**) (Top) Representative peak-height histograms of smFISH spots from lysogenic (left, red, NK7049 λ_{WT}, N = 45089), P_{RM} reporter (right, red, AP365, N = 58443), and negative samples lacking the target mRNA (black, NK7049, N = 8180 and 8146, respectively), labeled using IF-smFISH. As in the case of smFISH alone (**fig. S8**), the histograms of the positive samples show two well separated peaks, corresponding to bona fide spots (right peak) and spots due to the non-specific binding of probes (left peak). (Bottom) mRNA spot intensity histograms for the positive samples shown above, considering only bona fide spots (lysogen, N = 4847; P_{RM} reporter, N = 16849). As in the case of smFISH alone (**fig. S8**), the mRNA spot intensity histograms (red markers, error bars are SEM for each bin) are well described by a sum of multiple Gaussian functions (black), corresponding to the expected fluorescence of spots containing 1 to 3 mRNAs (shaded red areas). (**E**) Estimated number of cI mRNA per lysogen (NK7049 λWT) and lacZ mRNA per P_{RM} reporter (AP327, no CI) obtained using smFISH or IF-smFISH labeling (red). The estimates are the mean ± SD for 3554 cells, or the number of samples shown in parenthesis.

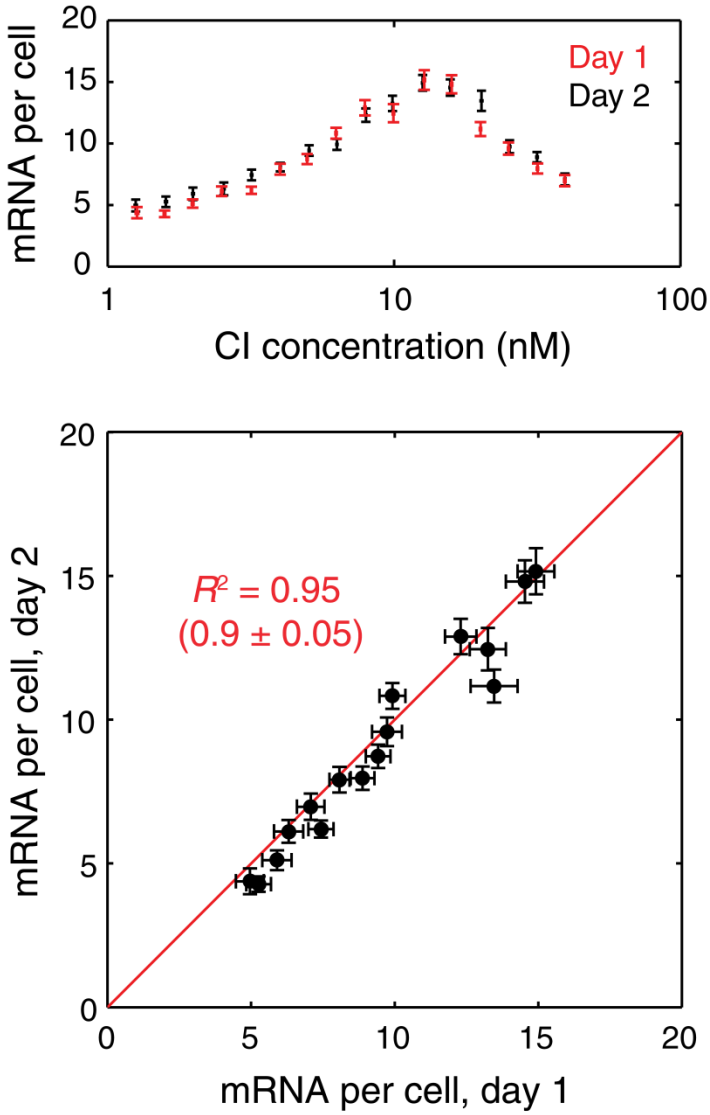

Fig. S11: Reproducibility of the P_{RM}(CI) regulation curve.

(Top) Two IF-smFISH measurements of the O_L^+ P_{RM} reporter (AP365, N = 2889 and 3270 cells) performed in consecutive days were analyzed and the regulation curve of each experiment was calculated by averaging over finite windows of CI concentration (red and black, error bars are SEM for bins with > 40 cells). The protein concentration of one of the curves was scaled to maximize the agreement between the mRNA expression levels of both curves (the scaling factor for the curves shown is 0.68, the mean ± SD for 3 independent comparisons is 0.82 ± 0.12). (Bottom) Comparison of the mean mRNA levels (black, error bars are SEM) for bins of different CI concentration, from the curves shown above. The R^2 between the data and the y = x line is shown in red. The value in parenthesis is the mean ± SD of the R^2 for 3 independent comparisons (6 experiments, N = 553 to 3270 cells).

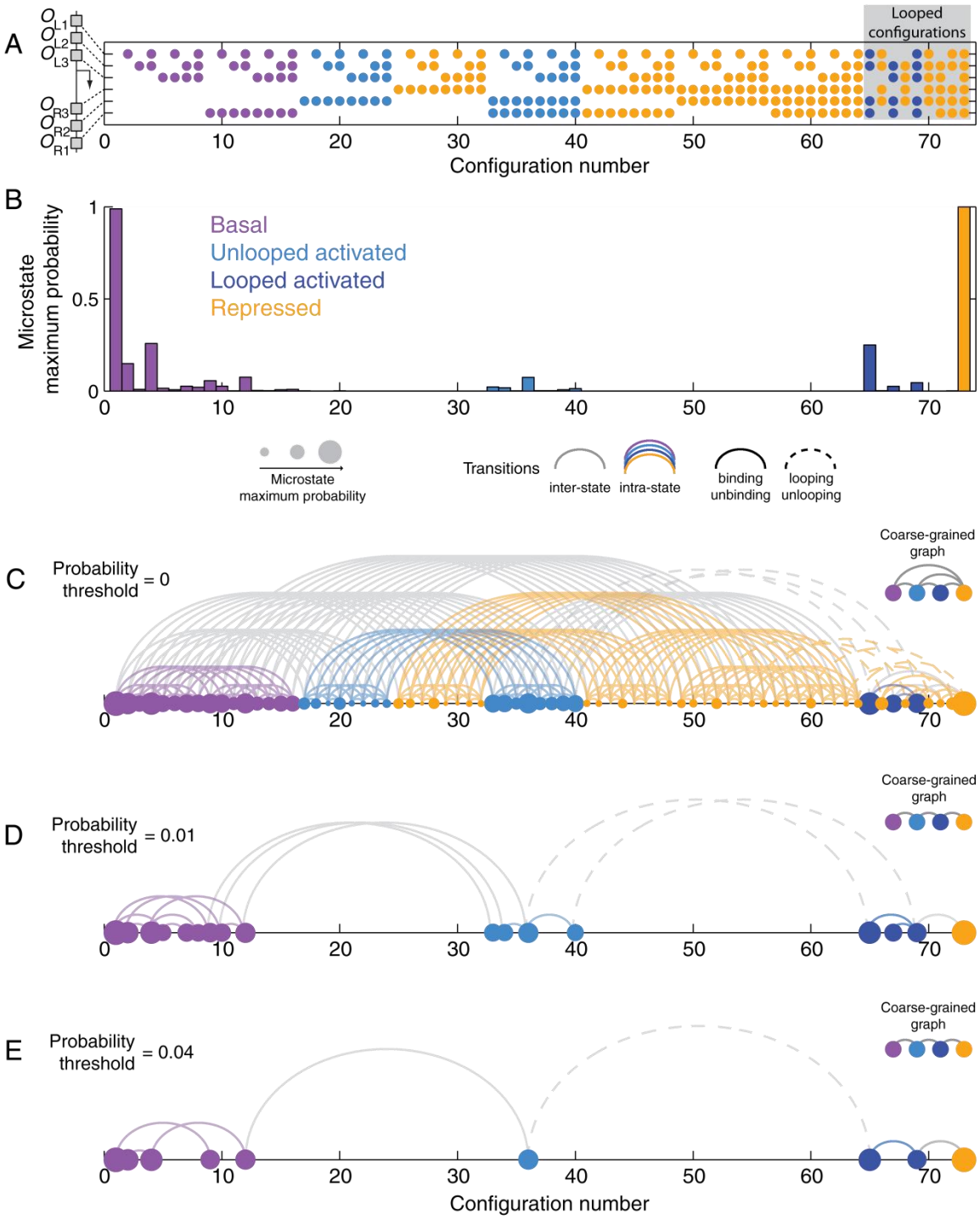

Fig. S12: Modeling P_{RM} regulation.

(**A**) CI binding and DNA looping configurations, defining the microstates of the P_{RM} promoter (following (*15*)). The promoter can adopt 73 microstates, 64 of which are unlooped and 9 are looped (gray background). Each microstate is colored according to its expected transcriptional activity (purple, basal; cyan, unlooped activated; blue, looped activated; orange, repressed). (**B**) The probability of observing each of the P_{RM}

microstates, maximized over all CI concentrations. The probabilities were calculated using the thermodynamic model described in **section 3.1**. (**C**-**E**) Coarse-graining used to define the stochastic model. (**C**) Arc diagram describing the possible transitions between P_{RM} microstates. A transition is allowed if it involves (i) the binding/unbinding of a single CI dimer, or (ii) looping/unlooping of the promoter while keeping the CI binding state unmodified. Transitions within the same activity level are shown in color, whereas transitions between activity levels are shown in gray. Transitions involving the binding/unbinding of CI dimers are shown as solid lines, whereas transitions involving looping/unlooping are shown as dashed lines. The radius of each node in the diagram is proportional to the logarithm of the maximal probability of the state (see panel B). The inset (right) shows the corresponding coarse-grained transition diagram, where two transcriptional activity levels (macrostates) are linked if there is at least one allowed transition between them. This transition diagram is branched rather than linear. Each transition in the coarse-grained diagram may represent a series of transitions between microstates, which have the net effect of switching the promoter from one activity level to another. (**D**) To simplify the model, we excluded microstates that never reach a probability >1% at any CI concentration. The resulting coarse-grained transition diagram (inset) is now linear (basal ↔ unlooped activated ↔ looped activated ↔ repressed). However, transitions between activity levels may still correspond to a series of multiple microscopic transitions. (**E**) To simplify the model further, we next excluded microstates that never reach a probability > 4%. The resulting coarse-grained transition diagram (inset) is still linear, with the added property that the transitions between promoter activity levels now correspond to unique transitions between microstates.

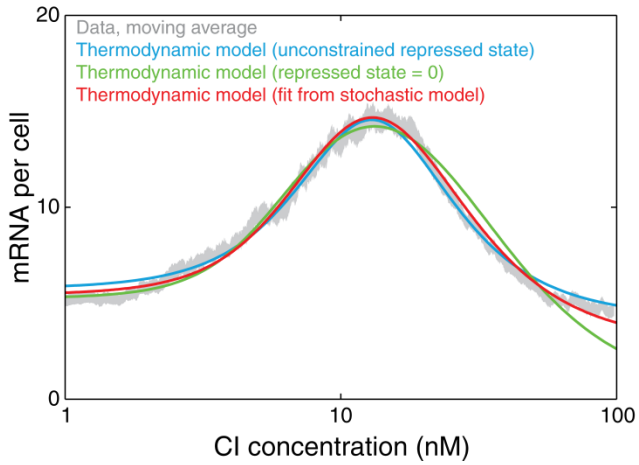

Fig. S13: Comparing different theoretical fits to the experimental data.

A moving average (200 cells per bin) of the measured mRNA level from a representative P_{RM}(CI) regulatory curve (gray, mean ± SEM) is overlaid with the results from the fit to the thermodynamic model without (cyan, R^2 = 0.981), and with (green, R^2 = 0.970) a constraint on the activity of the repressed state. Also shown is the thermodynamic model using the parameters obtained from the fit to the stochastic model (red, R^2 = 0.987). Calculating R^2 using different bins did not affect the rank order of R^2 for the three fitting methods.

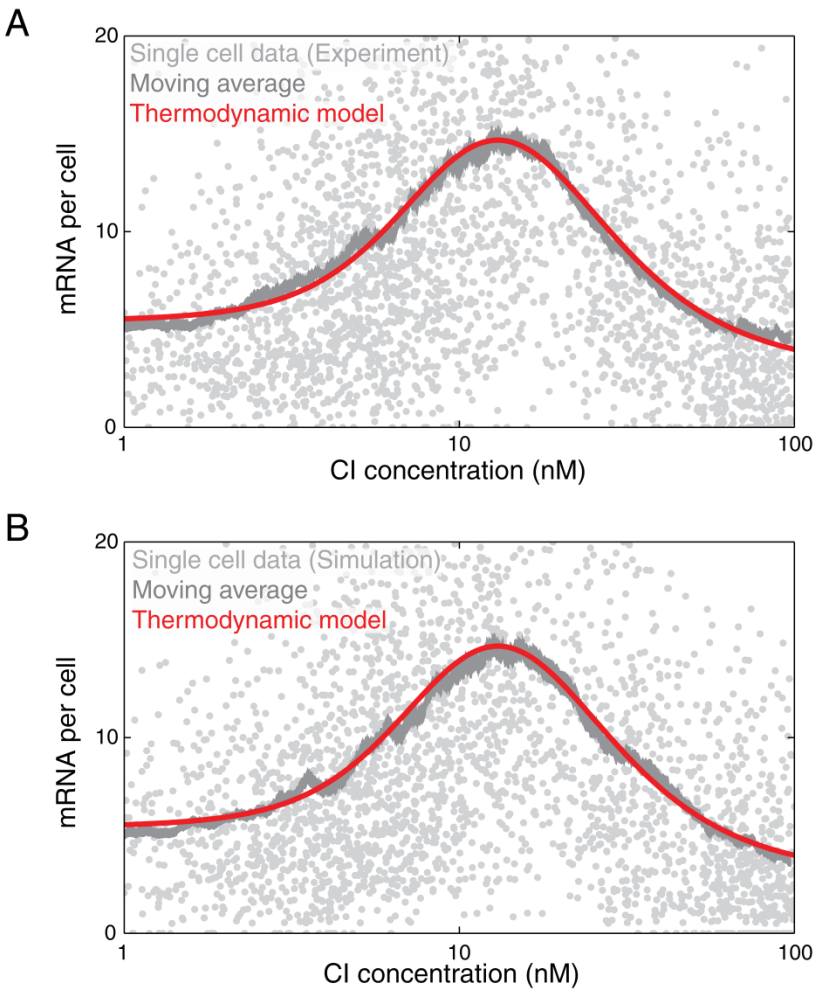

Fig. S14 Simulating the single-cell protein/mRNA data.

(**A**) The experimental single-cell data from the P_{RM} reporter (AP365) reproduced from **Fig. 4C**. (**B**) Simulated single-cell data, obtained from the stochastic model. For each cell in the experimental data set (total of 2941), we used the stochastic model (see **section 3.2**) to calculate the expected probability distribution for the number of mRNAs/cell. This distribution was used to generate a single simulated data point, (CI concentration, number of mRNA/cell). To simulate mRNA counting errors, we added a random number in the range [-0.5,0.5] to each mRNA value. Any negative mRNA value was rounded to zero. Both the experimental and simulated datasets were filtered using a moving average (dark gray, 200 cells/bin). Also shown are the results from the thermodynamic fit (red).

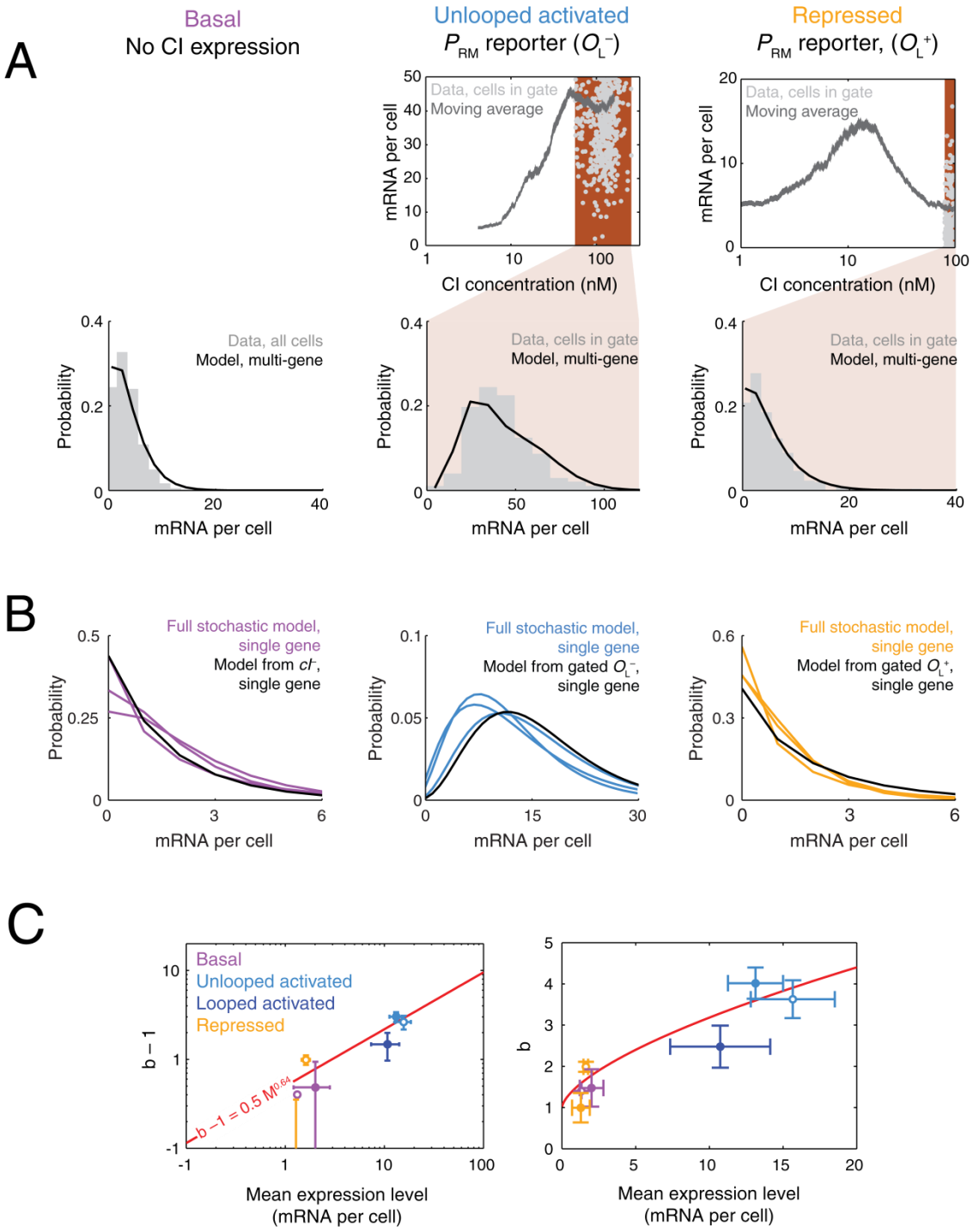

Fig. S15: Genetic controls and parameter estimates for P_{RM} activity.

(**A**) To estimate the kinetic parameters of the unlooped activated (center) and repressed (right) promoter states, we defined high-CI concentration gates (brown areas, N = 578 and 260 cells, respectively) in the measured regulatory curves of the O_L^- and O_L^+ P_{RM} reporters (top, dark gray curves are the mean ± SEM of a moving average) and fitted the mRNA copy number distribution in each of the gates to the model $P = \alpha P(m; 2r, p) +$ (1

– α)$P(m; 4r, p)$ (black) where $P(m; r, p)$ is a negative binomial distribution with parameters r (the burst frequency) and p (related to the burst size b via $b = (1 – p)/p$), and α is the fraction of cells with 2 copies of the P_{RM} promoter (see **section 2.5.2**). The kinetic parameters for the basal state (left) were similarly estimated from the measured mRNA statistics of a P_{RM} reporter with no CI expression (N = 1012 cells). (**B**) The mRNA distributions, corresponding to a single gene copy, for the basal, activated unlooped and repressed states. The distributions were calculated from the estimated parameters of the stochastic model for three independent experiments (colored curves, N = 706, 2600 and 2941 cells). Also shown (black curves) are the single-gene distributions corresponding to the data sets from panel A. (**C**) Transcription parameters for the different single-gene promoter states obtained from the stochastic model (solid circles) and the genetic controls (empty circles). Shown is the burst size b as a function of the mean expression level. Error bars are SEM over 3 independent experiments. Shown in red is the observed relationship between burst size and expression level described in (*29*). Left, log-log scale. Right, linear scale.

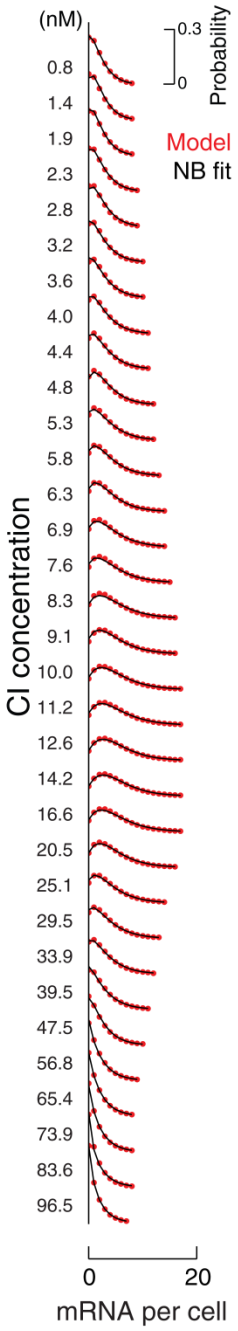

Fig. S16 The calculated single-gene histograms from the stochastic model.

The single-gene histograms corresponding to the mRNA distributions shown in **Fig. 4F** (red). These distributions were well fitted by a negative binomial (NB) distribution (black), indicating simple bursty kinetics.

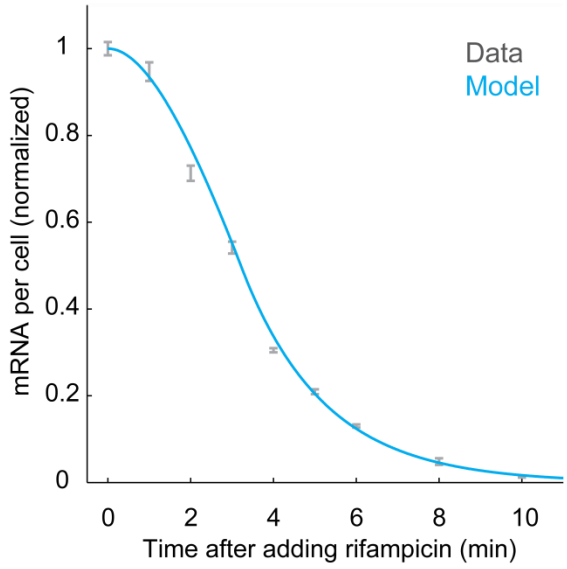

Fig. S17 Using smFISH to measure mRNA kinetics following rifampicin treatment.
Cells (strain TK310, described in (*45*)) were grown at 37 °C in M9 medium + casamino acids + glucose (Teknova), in the presence of 1 mM IPTG and 1 mM cAMP to achieve full induction of the lac promoter. When the culture reached OD600 = 0.2, transcription initiation was inhibited by adding rifampicin to a final concentration of 500 ug/ml (*34*). At the indicated time points, cells were fixed and labeled for lacZ mRNA using smFISH as described in (*25*). The cell-averaged mRNA level, normalized by the first time point (gray, mean ± SEM from 1000-3000 cells each) is plotted as a function of time. The data was fitted to the theoretical model of (*35*), using the following parameters: gene length, L = 7000 base pairs; degradation rate k_d = 1/120 s^{-1}; transcription elongation speed v_{El} = 15.5 nucleotides/sec.

Table S1 Bacterial strains used in this work.

Strain	Relevant genotype	Plasmids	Measured species	Reference
NK7049 *Negative control for P_{RM} reporter*	λ^-, Δ*lacIZYA*	-	-	Dodd *et al.* (2004)[1]
NK7049 λ_{WT}[2] *lambda lysogen*	λ^+	-	*cI* mRNA, CI protein	Dodd *et al.* (2004)[1]
MG1655 λ_{831}[2] *lambda lysogen*	λ^+	-	CI protein	Lab stock
AP365 *P_{RM} reporter*	λRS45Δ*lacYA*-P_{RM}::*lacZ*, O_L^+, *cro*$^-$	pUHA1(Kan^R) pZC320-*cI*(Amp^R)	*lacZ* mRNA, CI protein	Dodd *et al.* (2004)[1]
AP327 *P_{RM} reporter (no CI, used as control for basal state estimates)*	λRS45Δ*lacYA*-P_{RM}::*lacZ*, O_L^-, *cro*$^-$	pUHA1(Kan^R) pZC320(Amp^R)	*lacZ* mRNA	Dodd *et al.* (2004)[1]
AP326 *P_{RM} reporter (O_L^-*, used as control for *unlooped activated state estimates)*	λRS45Δ*lacYA*-P_{RM}::*lacZ*, O_L^-, *cro*$^-$	pUHA1(Kan^R) pZC320-*cI*(Amp^R)	*lacZ* mRNA, CI protein	Dodd *et al.* (2004)[1]
MG1655 *Negative control for CI-YFP reporter*	λ^-, Wild type	-	-	Lab stock
DH5αZ1 *CI-YFP reporter*	λ^-, *cI-yfp*$^+$	pZS21-*cIyfp*(Kan^R)	YFP, CI protein	Rosenfeld *et al.* (2004)[3]
LSG03 *galK locus reporter*	λ^-, Δ*galK*::*tetO*$_{140}$, Gen^R	pDM21-*tetRyfp*(Kan^R)	YFP	This work[4]

[1]Gift from K. Shearwin, University of Adelaide.
[2]Monolysogeny (the presence of a single lambda prophage per bacterial chromosome) was verified using PCR following the method of (*46*).
[3]Gift from M. Elowitz, California Institute of Technology.
[4]LSG03 was created by moving an array of 140 *tetO* sites from BW25113 Δ*galK*::*tetO*$_{140}$ (lab stock) to NK7049 using P1 transduction, and transforming the resulting strain with the pDM21-*tetRyfp* plasmid (*27*)(a gift from D. Bates, Baylor College of Medicine). LSG03 grew with the same generation time (30.5 ± 1.1 min) as NK7049 λ_{WT} (31.0 ± 0.3 min).

Table S2 Literature estimates for the number of CI molecules in a lysogen.

Reference	CI monomers per lysogen	Method	Medium	T (°C)	Strain
Hensel *et al.* (2012)	140	Single-molecule quantification of fluorescent fusion protein	M9A	37	MG1655
Levine *et al.* (1979)	280[1]	Capture of DNA-bound repressor to nitrocellulose filter	BT	37	GY3639
Reichardt *et al.* (1971)	225[2]	Capture of DNA-bound repressor to nitrocellulose membranes, immunolabeling	TY	30,42	W3350

[1]Reported value is 140 molecules of the active repressor (the species that binds to DNA).
[2]The authors report that a lysogen produces 3.75 CI monomers per minute, and that the generation time is 40 min. Therefore, a lysogen produces a total of 3.75 CI/min × 40 min = 150 CI monomers in one cell cycle. Assuming that CI is not actively degraded, the average number of monomers per lysogen is ≈225.

Table S3 P_{RM} parameters estimated from CI protein copy-number statistics in a lysogen.

	Bursts per cell generation (a_{CI})[1]	Proteins per burst (b_{CI})[1]	Bursts per min (f_{CI})[2]	Proteins per mRNA[3]	CI proteins per cell[4]
Lysogen, whole population	8.9 ± 0.6	21 ± 4	0.29 ± 0.02	6.38 ± 3.12	186 ± 8

[1]Parameters a_{CI} and b_{CI} were obtained by fitting the protein copy-number histogram (**Fig. 2E**) to a gamma distribution. Error bars are SEM over 7 experiments (99 to 883 cells per experiment).
[2]Calculated as $f_{CI} = r_{CI} / \tau_g$, where τ_g is the cell generation time (30.5 ± 0.1 min).
[3]Calculated as b_{CI} / b_{cI}, where b_{cI} is the number of mRNA per burst (**table S4**)
[4]Average of estimates from spot and fluctuation methods (**Fig. 2E**).

Table S4: P_{RM} parameters obtained from *cI* mRNA copy-number statistics in a lysogen.

	Burst per mRNA lifetime (r_{cI})[1]	mRNA per burst (b_{cI})[1]	Burst per min (f_{cI})[2]	*cI* mRNA per cell
Lysogen, single gene	0.72 ± 0.16	3.29 ± 0.95	0.18 ± 0.04	2.4
Lysogen, whole population[3]	1.47 ± 0.05	3.87 ± 0.12	0.37 ± 0.01	5.7 7.8 ± 0.7[4]

[1] r_{cI} and b_{cI} were obtained as described in **section 2.6**.
[2] Calculated as $f_{cI} = r_{cI} / \tau_{cI}$, where is the lifetime of the *cI* mRNA (4.0 ± 0.8 min, (*23*)).
[3] Obtained by fitting the whole-population mRNA data (**Fig. 3A**) (considering cells between percentiles 5 and 95 in cell length) to a negative binomial distribution.
[4] All cells in the population, no gating by length. Mean ± SD of 2 experiments.

Table S5: Parameters used in the thermodynamic model of P_{RM} regulation.

Fixed parameters[1]		Fitted parameters[2]				
			Dodd et al. (2004)	unconstrained repressed state	repressed state = 0	fit from stochastic model
Parameter[1]	**Value**	**Parameter**	**Value**	**Value**	**Value**	**Value**
$\Delta G_{O_{R1}}$	-13.2 kcal/mol	ΔG_{Oct}	-0.5 kcal/mol	-1.1 ± 0.5 kcal/mol	-1.1 ± 0.5 kcal/mol	-0.7 ± 0.3 kcal/mol
$\Delta G_{O_{R2}}$	-10.7 kcal/mol	ΔG_{Tet}	-3.0 kcal/mol	-3.9 ± 0.2 kcal/mol	-3.9 ± 0.2 kcal/mol	-4.4 ± 0.2 kcal/mol
$\Delta G_{O_{R3}}$	-10.2 kcal/mol	K_{NS}	$2.4 \cdot 10^4$ M^{-1} [3]	4187 ± 253 M^{-1}	4031 ± 109 M^{-1}	4122 ± 328 M^{-1}
$\Delta G_{O_{L1}}$	-13.8 kcal/mol	M_B	45 LacZ units	4.7 ± 0.9 mRNA	4.6 ± 0.6 mRNA	4.7 ± 0.6 mRNA
$\Delta G_{O_{L2}}$	-12.1 kcal/mol	M_U	360 LacZ units	43.1 ± 4.7 mRNA	29.7 ± 3.9 mRNA	36.0 ± 4.8 mRNA
$\Delta G_{O_{L3}}$	-12.4 kcal/mol	M_R	0.5 LacZ units	3.3 ± 1.0 mRNA	N/A	2.8 ± 0.1 mRNA
$\Delta G_{Adj}^{O_R}$	-3 kcal/mol	M_U / M_B	8	9.2 ± 2.0	6.5 ± 1.2	7.7 ± 1.4
$\Delta G_{Adj}^{O_L}$	-2.5 kcal/mol					
K_{Dim}	$6.7 \cdot 10^{-7}$ M^{-1}					
[NS]	$6.76 \cdot 10^{-3}$ M					

[1]Parameters held constant during the fitting procedure. The values were taken from (*15*), see **section 3.1**.
[2]Parameters fitted to the experimental data. Values are mean ± SD from 3 experiments. The curves corresponding to these parameters are shown in **fig. S13**.
[3] K_{NS} obtained by Dodd et al. was an arbitrary scaling factor to compare *in vitro* and *in vivo* data.

Table S6: Estimated parameters for the different P_{RM} activity states, obtained from the reporter system.

Promoter state	Bursts per mRNA lifetime (r)[1]	mRNA per burst (b)[1]	Bursts per min (f)[2]	Mean mRNA per cell
Fits to P_{RM} curve (single gene)[3]				
Basal	1.36 ± 0.6	1.47 ± 0.79	0.68 ± 0.3	1.71 ± 0.21
Unlooped activated	3.27 ± 0.6	4.02 ± 0.66	1.63 ± 0.3	12.94 ± 1.71
Looped activated	4.33 ± 1.8	2.48 ± 0.88	2.17 ± 0.9	9.70 ± 1.28
Repressed	1.29 ± 0.68	1.00 ± 0.62	0.64 ± 0.34	1.01 ± 0.05
Fits to genetic controls (single gene)[4]				
Basal	0.94 ± 0.01	1.40 ± 0.01	0.47 ± 0.01	1.32 ± 0.01
Unlooped activated	4.32 ± 0.56	3.63 ± 0.46	2.1 ± 0.28	15.66 ± 2.85
Repressed	0.81 ± 0.06	1.99 ± 0.12	0.41 ± 0.03	1.62 ± 0.15

[1] r and b for each of the single-gene promoter states were obtained by fitting the stochastic model in **section 3.2** to the P_{RM} reporter data.
[2] Calculated as $f = r / \tau_{lacZ}$ where τ_{lacZ} is the lifetime of the *lacZ* mRNA (2.0 ± 0.1 min, (*29*)).
[3] Mean ± SEM of the parameters obtained from fits to three independent experiments (N = 553 to 3270 cells experiment).
[4] r and b for each of the single-gene promoter states were obtained from fitting the stochastic model in **section 2.6** to the mRNA copy-number histograms of the genetic controls (N = 260 to 1012 cells per experiment, **fig. S15A**).

Movie S1

Shown is the fit of the stochastic model to P_{RM}(CI) single-cell data. Each frame of the movie shows the mRNA copy-number histogram at a particular CI concentration (gray, N = 100 cells per frame), overlaid with the prediction of the stochastic model (red). The part of the P_{RM} curve corresponding to the histogram is shown in the inset.

Supplementary caption for Fig. 1

(A) The P_{RM} regulatory curve. The curve (gray line) was generated using the model and parameters described in (*15*). The colored shaded regions indicate CI concentrations where the different promoter states (basal, activated and repressed; in purple, blue and orange, respectively) have a calculated probability higher than 0.3. The vertical shaded area is centered on the expected concentration of the lambda lysogen ($3.7 \cdot 10^{-7}$ M, (*15*)). At that CI concentration, the P_{RM} promoter is expected to spend 6% of the time in the basal state, 60% in the activated state, and 34% in the repressed state. **(B)** Simulating the transcriptional time series and mRNA copy number distribution of the lambda lysogen. To test the effect of promoter-state switching, we modeled the lysogen using simple two-state stochastic switching between the activated and repressed states, with the P_{RM} promoter in the active state is 60% of the time, and in the repressed state 40% of the time. mRNA was produced from the activated and repressed states with Poissonian rates k_{TX1} = 0.005 s^{-1} and k_{TX2} = 0.1 s^{-1}, respectively, while mRNA was degraded with rate k_d = 0.008 s^{-1} (a lifetime of 2 min, the measured value for *lacZ* mRNA used in the reporter system (*29*)). Depending on the relative switching rate between the states, the two-state model will show distinct behaviors. We used Gillespie simulations (*47*) and the Finite State Projection algorithm (*42*) to generate representative transcriptional time series (top) and mRNA statistics (center and bottom) in the limits of slow ($k_{Act \rightarrow Rep}$ = $6.6 \cdot 10^{-5}$ s^{-1} and $k_{Rep \rightarrow Act}$ = $1 \cdot 10^{-4}$ s^{-1}) and fast ($k_{Act \rightarrow Rep}$ = 6.6 s^{-1} and $k_{Rep \rightarrow Act}$ = 10 s^{-1}) switching. In the slow switching limit, the dwell time in each state is long, making each state easily discernable both in the transcriptional time series and mRNA statistics. Conversely, in the fast switching limit, both the time series and the resulting mRNA statistics show a single effective state.

References

1. B. Pulverer, Getting specific. *Nat. Rev. Mol. Cell. Biol.* **6**, S12-S13 (2005).

2. M. Ptashne, A. Gann, *Genes & signals*. (Cold Spring Harbor Laboratory Press, Cold Spring Harbor, N.Y., 2002).

3. E. H. Davidson, M. S. Levine, Properties of developmental gene regulatory networks. *Proc. Natl. Acad. Sci. U. S. A.* **105**, 20063-20066 (2008).

4. L. M. Anderson, H. Yang, DNA looping can enhance lysogenic CI transcription in phage lambda. *Proc. Natl. Acad. Sci. U. S. A.* **105**, 5827-5832 (2008).

5. L. Cui, I. Murchland, K. E. Shearwin, I. B. Dodd, Enhancer-like long-range transcriptional activation by lambda CI-mediated DNA looping. *Proc. Natl. Acad. Sci. U. S. A.* **110**, 2922-2927 (2013).

6. E. H. Davidson, *The regulatory genome : gene regulatory networks in development and evolution*. (Academic, Burlington, MA; San Diego, 2006).

7. M. Ptashne, *A genetic switch*. (Cold Spring Harbor Laboratory Press, Cold Spring Harbor, Nerw York, 2004).

8. A. Eldar, M. B. Elowitz, Functional roles for noise in genetic circuits. *Nature* **467**, 167-173 (2010).

9. A. Sanchez, I. Golding, Genetic determinants and cellular constraints in noisy gene expression. *Science* **342**, 1188-1193 (2013).

10. M. J. Levesque, P. Ginart, Y. Wei, A. Raj, Visualizing SNVs to quantify allele-specific expression in single cells. *Nat. Methods* **10**, 865-867 (2013).

11. M. A. Shea, G. K. Ackers, The OR control system of bacteriophage lambda. A physical-chemical model for gene regulation. *J. Mol. Biol.* **181**, 211-230 (1985).

12. E. Segal, T. Raveh-Sadka, M. Schroeder, U. Unnerstall, U. Gaul, Predicting expression patterns from regulatory sequence in *Drosophila* segmentation. *Nature* **451**, 535-540 (2008).

13. D. L. Jones, R. C. Brewster, R. Phillips, Promoter architecture dictates cell-to-cell variability in gene expression. *Science* **346**, 1533-1536 (2014).

14. I. B. Dodd, A. J. Perkins, D. Tsemitsidis, J. B. Egan, Octamerization of lambda CI repressor is needed for effective repression of P(RM) and efficient switching from lysogeny. *Genes. Dev.* **15**, 3013-3022 (2001).

15. I. B. Dodd, K. E. Shearwin, A. J. Perkins, T. Burr, A. Hochschild, J. B. Egan, Cooperativity in long-range gene regulation by the lambda CI repressor. *Genes. Dev.* **18**, 344-354 (2004).

16. N. Rosenfeld, J. W. Young, U. Alon, P. S. Swain, M. B. Elowitz, Gene regulation at the single-cell level. *Science* **307**, 1962-1965 (2005).

17. K. S. Koblan, G. K. Ackers, Energetics of subunit dimerization in bacteriophage lambda cI repressor: linkage to protons, temperature, and KCl. *Biochemistry* **30**, 7817-7821 (1991).

18. H. Xu, L. A. Sepúlveda, L. Figard, A. M. Sokac, I. Golding, Combining protein and mRNA quantification to decipher transcriptional regulation. *Nat. Methods.* **12**, 739-742 (2015).

19. Z. Hensel, H. Feng, B. Han, C. Hatem, J. Wang, J. Xiao, Stochastic expression dynamics of a transcription factor revealed by single-molecule noise analysis. *Nat. Struct. Mol. Biol.* **19**, 797-802 (2012).

20. A. Levine, A. Bailone, R. Devoret, Cellular levels of the prophage lambda and 434 repressors. *J. Mol. Biol.* **131**, 655-661 (1979).

21. L. Reichardt, A. D. Kaiser, Control of lambda repressor synthesis. *Proc. Natl. Acad. Sci. U. S. A.* **68**, 2185-2189 (1971).

22. N. Friedman, L. Cai, X. S. Xie, Linking stochastic dynamics to population distribution: an analytical framework of gene expression. *Phys. Rev. Lett.* **97**, 168302 (2006).

23. C. Zong, L. H. So, L. A. Sepúlveda, S. O. Skinner, I. Golding, Lysogen stability is determined by the frequency of activity bursts from the fate-determining gene. *Mol. Syst. Biol.* **6**, 440 (2010).

24. A. Raj, P. van den Bogaard, S. A. Rifkin, A. van Oudenaarden, S. Tyagi, Imaging individual mRNA molecules using multiple singly labeled probes. *Nat. Methods* **5**, 877-879 (2008).

25. S. O. Skinner, L. A. Sepúlveda, H. Xu, I. Golding, Measuring mRNA copy number in individual *Escherichia coli* cells using single-molecule fluorescent in situ hybridization. *Nat. Protoc.* **8**, 1100-1113 (2013).

26. K. Nordstrom, S. Dasgupta, Copy-number control of the *Escherichia coli* chromosome: a plasmidologist's view. *EMBO Rep.* **7**, 484-489 (2006).

27. M. C. Joshi, A. Bourniquel, J. Fisher, B. T. Ho, D. Magnan, N. Kleckner, D. Bates, *Escherichia coli* sister chromosome separation includes an abrupt global transition with concomitant release of late-splitting intersister snaps. *Proc. Natl. Acad. Sci. U. S. A.* **108**, 2765-2770 (2011).

28. D. Lewis, P. Le, C. Zurla, L. Finzi, S. Adhya, Multilevel autoregulation of lambda repressor protein CI by DNA looping in vitro. *Proc. Natl. Acad. Sci. U. S. A.* **108**, 14807-14812 (2011).

29. L. H. So, A. Ghosh, C. Zong, L. A. Sepúlveda, R. Segev, I. Golding, General properties of transcriptional time series in *Escherichia coli*. *Nat. Genet.* **43**, 554-560 (2011).

30. C. Manzo, C. Zurla, D. D. Dunlap, L. Finzi, The effect of nonspecific binding of lambda repressor on DNA looping dynamics. *Biophys J.* **103**, 1753-1761 (2012).

31. Z. Hensel, X. Weng, A. C. Lagda, J. Xiao, Transcription-factor-mediated DNA looping probed by high-resolution, single-molecule imaging in live *E. coli* cells. *PLoS Biol.* **11**, e1001591 (2013).

32. A. Coulon, C. C. Chow, R. H. Singer, D. R. Larson, Eukaryotic transcriptional dynamics: from single molecules to cell populations. *Nat. Rev. Genet.* **14**, 572-584 (2013).

33. P. Hammar, M. Wallden, D. Fange, F. Persson, O. Baltekin, G. Ullman, P. Leroy, J. Elf, Direct measurement of transcription factor dissociation excludes a simple operator occupancy model for gene regulation. *Nat. Genet.* **46**, 405-408 (2014); published online EpubApr (10.1038/ng.2905).

34. J. A. Bernstein, A. B. Khodursky, P. H. Lin, S. Lin-Chao, S. N. Cohen, Global analysis of mRNA decay and abundance in Escherichia coli at single-gene resolution using two-color fluorescent DNA microarrays. *Proc. Natl. Acad. Sci. U. S. A.* **99**, 9697-9702 (2002).

35. H. Chen, K. Shiroguchi, H. Ge, X. S. Xie, Genome-wide study of mRNA degradation and transcript elongation in Escherichia coli. *Mol. Syst. Biol.* **11**, 781 (2015).

36. J. Buss, C. Coltharp, J. Xiao, Super-resolution imaging of the bacterial division machinery. *J. Vis. Exp.*, (2013).

37. J. W. Young, J. C. Locke, A. Altinok, N. Rosenfeld, T. Bacarian, P. S. Swain, E. Mjolsness, M. B. Elowitz, Measuring single-cell gene expression dynamics in bacteria using fluorescence time-lapse microscopy. *Nat. Protoc.* **7**, 80-88 (2012).

38. B. Zhang, J. Zerubia, J. C. Olivo-Marin, Gaussian approximations of fluorescence microscope point-spread function models. *Appl. Opt.* **46**, 1819-1829 (2007).

39. A. Raj, C. S. Peskin, D. Tranchina, D. Y. Vargas, S. Tyagi, Stochastic mRNA synthesis in mammalian cells. *PLoS Biol.* **4**, e309 (2006).

40. K. Bahar Halpern, S. Tanami, S. Landen, M. Chapal, L. Szlak, A. Hutzler, A. Nizhberg, S. Itzkovitz, Bursty gene expression in the intact mammalian liver. *Mol. Cell.* **58**, 147-156 (2015); published online EpubApr 2 (

41. G. Neuert, B. Munsky, R. Z. Tan, L. Teytelman, M. Khammash, A. van Oudenaarden, Systematic identification of signal-activated stochastic gene regulation. *Science* **339**, 584-587 (2013).

42. B. Munsky, M. Khammash, The finite state projection algorithm for the solution of the chemical master equation. *J. Chem. Phys.* **124**, 044104 (2006); published online EpubJan 28 (

43. F. C. Neidhardt, *Escherichia coli and Salmonella typhimurium: cellular and molecular biology*. (American Society for Microbiology, Washington, D.C., 1987).

44. T. E. Kuhlman, E. C. Cox, Gene location and DNA density determine transcription factor distributions in Escherichia coli. *Mol. Syst. Biol.* **8**, 610 (2012).

45. T. Kuhlman, Z. Zhang, M. H. Saier, Jr., T. Hwa, Combinatorial transcriptional control of the lactose operon of Escherichia coli. *Proc. Natl. Acad. Sci. U. S. A.* **104**, 6043-6048 (2007).

46. B. S. Powell, M. P. Rivas, D. L. Court, Y. Nakamura, C. L. Turnbough, Jr., Rapid confirmation of single copy lambda prophage integration by PCR. *Nucleic Acids Res.* **22**, 5765-5766 (1994).

47. D. Gillespie, A General Method to Numerically Simulating the Stochastic Time Evolution of Coupled Chemical Reactions *J. Comp. Phys.* **22**, 403-434 (1976).